Author(s): Melander, Marko; Kuisma, Mikael; Christensen, Thorbjørn Erik Køppen; Honkala, Karoliina

Title: Grand-canonical approach to density functional theory of electrocatalytic systems: Thermodynamics of solid-liquid interfaces at constant ion and electrode potentials

Year: 2019

Version: Published version

Please cite the original version:

Melander, M., Kuisma, M., Christensen, T. E. K., & Honkala, K. (2019). Grand-canonical approach to density functional theory of electrocatalytic systems: Thermodynamics of solid-liquid interfaces at constant ion and electrode potentials. Journal of Chemical Physics, 150(4), Article 041706. https://doi.org/10.1063/1.5047829

Grand-canonical approach to density functional theory of electrocatalytic systems: Thermodynamics of solid-liquid interfaces at constant ion and electrode potentials

Marko M. Melander, Mikael J. Kuisma, Thorbjørn Erik Køppen Christensen, and Karoliina Honkala

Grand-canonical approach to density functional theory of electrocatalytic systems: Thermodynamics of solid-liquid interfaces at constant ion and electrode potentials

Marko M. Melander,[1,a] Mikael J. Kuisma,[1] Thorbjørn Erik Køppen Christensen,[2] and Karoliina Honkala[1,b]

AFFILIATIONS

[1] Nanoscience Center, Department of Chemistry, University of Jyväskylä, P.O. Box 35 (YN), FI-40014 Jyväskylä, Finland
[2] Interdisciplinary Nanoscience Center (iNANO), Aarhus University, Gustav Wieds Vej 14 Building 1590, DK 8000 Aarhus C, Denmark

a) Electronic mail: marko.m.melander@jyu.fi
b) Electronic mail: karoliina.honkala@jyu.fi

ABSTRACT

Properties of solid-liquid interfaces are of immense importance for electrocatalytic and electrochemical systems, but modeling such interfaces at the atomic level presents a serious challenge and approaches beyond standard methodologies are needed. An atomistic computational scheme needs to treat at least part of the system quantum mechanically to describe adsorption and reactions, while the entire system is in thermal equilibrium. The experimentally relevant macroscopic control variables are temperature, electrode potential, and the choice of the solvent and ions, and these need to be explicitly included in the computational model as well; this calls for a thermodynamic ensemble with fixed ion and electrode potentials. In this work, a general framework within density functional theory (DFT) with fixed electron and ion chemical potentials in the grand canonical (GC) ensemble is established for modeling electrocatalytic and electrochemical interfaces. Starting from a fully quantum mechanical description of multi-component GC-DFT for nuclei and electrons, a systematic coarse-graining is employed to establish various computational schemes including (i) the combination of classical and electronic DFTs within the GC ensemble and (ii) on the simplest level a chemically and physically sound way to obtain various (modified) Poisson-Boltzmann (mPB) implicit solvent models. The detailed and rigorous derivation clearly establishes which approximations are needed for coarse-graining as well as highlights which details and interactions are omitted in vein of computational feasibility. The transparent approximations also allow removing some of the constraints and coarse-graining if needed. We implement various mPB models within a linear dielectric continuum in the GPAW code and test their capabilities to model capacitance of electrochemical interfaces as well as study different approaches for modeling partly periodic charged systems. Our rigorous and well-defined DFT coarse-graining scheme to continuum electrolytes highlights the inadequacy of current linear dielectric models for treating properties of the electrochemical interface.

Published by AIP Publishing. https://doi.org/10.1063/1.5047829

I. INTRODUCTION

Electrochemical reactions take place at the interface between electronic and ionic conductors (electrolyte). Together these two macroscopic conductors form an electrode, and electrochemical experiments probe the properties of this interface under the influence of applied voltage and current between electrodes. A typical current-voltage response obtained from an electrochemical experiment is often difficult to interpret from an atomistic perspective and

modeling is at the core of electrochemical analysis. Besides the reaction under study, the outcome of electrochemical experiments is controlled by the temperature, choice of electrolyte, and the electrode potential which determine the thermodynamic state of the system.[1] This scenario is depicted in Fig. 1.

The experimental setup sets the stage for a computational approach where macroscopic variables like the temperature and chemical potentials of the electrolyte and the electrode need to be controlled similarly as in the experiments. For macroscopic systems, the most natural thermodynamic ensembles at the thermodynamic limit are either the Gibbs $G(N, T, P)$ or the Helmholtz $A(N, T, V)$. The large number of species ensures that the, e.g., overall chemical potential of the electrolyte or electrode does not change during a reaction. For a small number of atoms as typically treated in a microscopic, atomistic simulation of the grand-canonical (GC) ensemble $\Omega(\mu, T, V)$ is a natural choice to allow treatment of a system at fixed chemical potentials with fluctuating particle numbers. Combining the experimental variables with the most widely used electronic structure method, density functional theory (DFT), motivates the development of grand canonical DFT (GC-DFT) to enable calculations at fixed chemical potentials and temperatures as performed in experiments.

GC-DFT offers a way to study electrochemical microscopic systems in thermodynamic equilibrium characterized by long time and length scales. If some parts of a system are prone to charge transfer events and chemical reactions, short time and small length-scales need to be included in the model. Thus, a general electrochemical model requires a quantum mechanical treatment of the electrode and reactants combined with a statistical treatment to capture changes in the interfacial charge distribution from the formation of
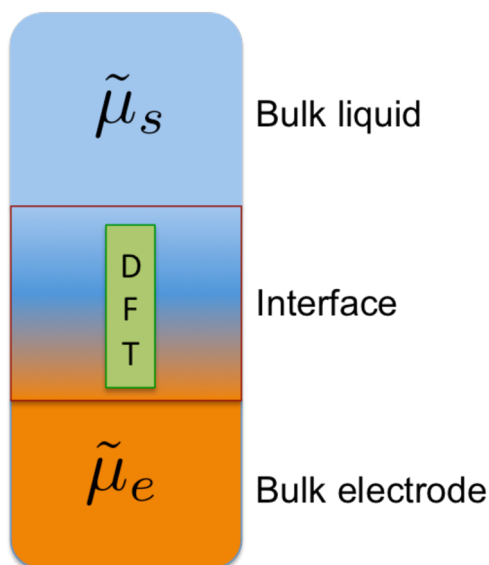
FIG. 1. The electrode-solvent interface in a grand-canonical picture where the solvent/electrolyte chemical potentials are fixed to $\tilde{\mu}_s$ and at the electrode the chemical potential of electrons is fixed to $\tilde{\mu}_n$.

the double-layer and liquid structure, for example. As the potential distribution controls reaction kinetics and thermodynamics, the electrolyte and its effect on the reacting system cannot be ignored. The mixture of several time scales and length scales and the need for a grand canonical description present serious challenges for the atomistic DFT models.

Need for constant ion and electrode potentials (grand canonical) rather than constant particle number treatment (canonical) is problematic for atomic-scale modeling and requires advanced simulation schemes.[2] In electronic GC-DFT, the electrode potential is controlled by the Fermi-level of the electrode which equals chemical potential of electrons, while the electrolyte chemical potential depends on the electrolyte solution and its concentration. Thus, a well-defined DFT model of an electrochemical interface calls for a GC ensemble with a fluctuating number of electrons and ions at a given temperature rather than the commonly applied canonical DFT where the particle number is fixed, but the chemical potentials are allowed to fluctuate.

To obtain equilibrium ensemble quantities from atomistic simulations, the most straight-forward solution is to adopt a statistical treatment of the system by using [ab initio or quantum mechanical/ molecular mechanical (QM/MM)] molecular dynamics (MD) where the reactants, electrode, and electrolyte are treated explicitly. To reach an equilibrium state, both the ionic and electronic degrees of freedom need to be sampled extensively. While this approach is well established[3–6] and justified, reaching equilibrium requires long simulations on large systems, making MD applicable to small systems and limited amount of reactions.

Another formally exact approach to model the thermodynamic ensemble effects is to use density functional theory where free energy of the entire system is defined in terms of the nuclear and electronic densities. After coarse-graining, classical parts can be fully described by atomic density distributions of different species.[7–9] Classical DFT is naturally formulated in the GC ensemble where the chemical potentials are fixed by the (pure) bulk phase. Like the classical DFT, also electronic GC-DFT can be realized.[10,11] By combining GC electronic and classical DFT, a unified DFT can be devised; previously this approach has been used to connect classical DFT with canonical DFT.[12–15]

In recent work, a classical/quantum DFT hybrid method suitable for periodic systems was obtained by combining electronic DFT with the reference interaction site method (RISM) of classical DFT.[15] When combined with the effective screening method (ESM),[16] the ESM-RISM was introduced. Using ESM-RISM with a potentiostat scheme[17] to control the electronic chemical potential within a few SCF cycles, a GC-DFT is achieved. Recently,[18] grand canonical electronic DFT has been combined with classical grand canonical description of the electrolyte. However, the steps needed to arrive in the separation between quantum and classical subsystems in the GC ensemble have not been addressed. In this work, we extend multi-component canonical electronic and nuclear DFT[19] to the grand canonical ensemble to provide a detailed route from

a fully quantum mechanical description to coarse-grained classical and continuum GC-DFT models of the electronic systems in contact with an electrolyte. This allows assessing the implications and omissions of different grand canonical DFT schemes.

The most elegant practical approach to electronic GC-DFT is to fix the Fermi-levels and allow the fluctuation of electrons during an SCF calculation. While stable algorithms for a constant electron potential (or Fermi-level) calculations have been developed recently,[18,20] the fluctuating number of electrons usually causes significant difficulties in practical calculations due to poor convergence. Another and equivalent way to obtain grand canonical averages is to perform calculations at several points using a fixed number of electrons and interpolate to the desired Fermi-level.[2,16,21–26] A more refined scheme based on constant number SCF calculations connects the electronic system to an additional degree of freedom, mimicking an artificial potentiostat which changes on the number of electrons in the system in order to achieve a predefined electrode potential.[17] Besides fixing the chemical potential of the electrons, also the chemical potential due to the solvent and ions needs to remain constant[22,23] which can be included in the quantum either mechanically or classically.

Changing the Fermi-level corresponds to changes in the electron chemical potential which is obtained by altering the charge state of the electrode. This presents a challenge for actual computations because electrocatalytic systems are usually partially periodic and periodic systems need to be charge neutral to avoid divergence of the electrostatic interactions. Typically a homogeneous back-ground charge is introduced, and various correction schemes have been devised[21,27,28] to relate charged and charge-neutral systems to a common reference. An elegant solution is provided by joint DFT (JDFT)[12,18,25] and (modified) Poisson-Boltzmann (mPB) implicit solvation models[29–31] where the charge neutrality can be maintained by the ionic distribution in the double-layer region. However, unlike commonly assumed, the charge neutrality constraint is not automatically fulfilled in non-linear mPB models,[32] which is most likely due to the over-simplified form of the mPB equations and the presence of the cavity exclusion function. Therefore, in practice, even the mPB models combined with electronic DFT as applied to charged periodic systems need to either enforce charge neutrality by using Lagrange multipliers,[32] use simple background charges,[33] or allow treatment of charged partially periodic systems by using modified mPB boundary conditions,[16] mimicking neutralization by image charges. These different ways of simulation charged periodic systems are investigated and compared in this work.

The mPB models present the simplest level of fixed potential GC-DFT of solid-liquid interfaces. Typically[23,25,29,31,34–36] the mPB models combine a linear dielectric implicit solvation model with an ion continuum following mPB distribution. The combination of DFT with mPB has been pursued by several groups, and various flavors of the methodology have been developed, implemented, and tested to treat electrochemical interfaces.[12,23,29,31] Most of these methods have been utilized in a linear dielectric to represent the liquid, while linearized, standard, and size-modified PB models have been used for describing the ions.[12,23,29,31] Typically, these models give reasonable agreement with solvation energies of neutral species but cannot reproduce electrochemically important experimental observables such as the double-layer capacitance. While it seems that the use of a non-linear dielectric improves the description of the solid-liquid interface,[37] the effect of adding more complexity to the description of the ion distribution has not yet been assessed; besides the general GC-DFT framework, one central question to answer in this work is to understand whether ion-specific interactions can improve the mPB description of solid-liquid interfaces.

In this paper, we present a formal way to study the properties of solid-liquid interfaces at fixed electrode and electrolyte chemical potentials by combining nuclear and electronic DFT within the grand canonical ensemble. The theory is turned into practical computational schemes by gradually coarse-graining the initially fully quantum mechanical description of both nuclei and electrons to (i) classical nuclei and (ii) eventually a continuum description of the solvent and ions. Besides a general framework, the detailed derivation of the electrochemical GC-DFT makes transparent approximations for particular computational models and highlights which details and interactions are omitted at different levels of theory. Understanding the details, omissions, and limitations of different GC-DFT models is highly important as the grand canonical approaches, especially the mPB models, are becoming more and more utilized in the computational studies of electrocatalytic reactions.

Within mPB models, we consider a general reference electrode to allow modeling at fixed absolute electrode potentials. We also review and develop practical computational schemes for modeling charged periodic systems. Finally, several standard and advanced mPB models within a linear dielectric approximation are implemented in the GPAW software and tested toward double layer capacitances and interfacial potential distributions. We show that adding varying amounts of ion-specific details in mPB models based on a linear dielectric does not improve the modeling of the double-layer capacitance nor significantly affect the potential distribution. Therefore, future work should concentrate on the development of non-linear dielectric mPB models or more refined classical DFT approaches. The developed GC-DFT hierarchy serves a basis for further developments of DFT approaches treating the electrochemical interfaces. In the future, the general framework will be extended to study electrochemical reactions and kinetics—work in this direction is already being made.

II. THEORY

A. Multi-component GC-DFT for electrochemical systems

Multi-component DFT (MCDFT)[19,38] provides a rigorous way to treat combined nuclear and electronic quantum

systems using DFT. In this work, MCDFT is extended into the grand canonical ensemble. The essential ingredients of the canonical MCDFT are presented in the supplementary material. While the canonical MCDFT approach is exact for the Helmholtz canonical free energy, typical systems treated within (electronic) DFT are very small due to the computational burden of such calculations. Even if the environment formed by the nuclei is treated classically, the systems are far from the thermodynamic limit. Therefore, in a microscopic simulation, the thermodynamic state characterized by macroscopic variables (such as the chemical potentials and temperature) of the system can change due to chemical reactions or fluctuations of the environment.[39] To describe equilibrium quantities of a small system in contact with an environment at fixed chemical potentials, it is more natural to fix the chemical potential of the environment rather than the particle number of the system. For a large enough system, both choices are naturally equivalent.

Fixing the chemical potential corresponds to a grand canonical ensemble. Performing a Legendre transformation in terms of the chemical potential on the canonical free energy gives the grand canonical Hamiltonian,[3]

$$\hat{\Omega} = \hat{H}_{tot} - T\hat{S}_{Nn} - \sum_i \tilde{\mu}_i \hat{N}_i, \qquad (1)$$

where total Hamiltonian is used and $\hat{H}_{tot} = \hat{T}_n + \hat{V}_{nn} + \hat{T}_N + \hat{V}_{Nn} + \hat{V}_{NN} + \sum_N \hat{V}_N + \sum_n \hat{v}_n$ with N for nuclei and n for electrons so that the grand canonical free energy is $\Omega = \Omega[T, V, \{\tilde{\mu}_i\}]$ specified by the (electro)chemical potentials $\tilde{\mu}_i$ and particle number operator $\hat{N}_i$. Now the particle number can fluctuate which leads to the following density operator:[3]

$$\hat{\rho}^{GC} = \frac{\exp[-\beta(\hat{H}_{tot} - \sum_i \tilde{\mu}_i \hat{N}_i)]}{\text{Tr}\left[\exp[-\beta(\hat{H}_{tot} - \sum_i \tilde{\mu}_i \hat{N}_i)]\right]}. \qquad (2)$$

We also define the partition function $\Xi = \text{Tr}\left[\exp\left[-\beta\left(\hat{H}_{tot} - \sum_i \mu_i \hat{N}_i\right)\right]\right]$ from which $\Omega[T, V, \mu] = -k_B T \ln \Xi = E - TS - \sum_i \mu_i N_i$. The probability of being in microstate i is

$$p_i^{GC} = \frac{\exp\left[-\beta\langle\Psi_i|\hat{H}_{tot} - \sum_j \tilde{\mu}_j \hat{N}_j |\Psi_i\rangle\right]}{\Xi}. \qquad (3)$$

In the above equation, $-\Psi_i\rangle$ is the total wave function of both the electrons and nuclei so that the particle number operators $\hat{N}_i$ correspond to electrons or the nuclear identities as specified below.

In the considered electrocatalytic framework as applied to a typical DFT calculation, the number of atoms at the electrode, number of solvent molecules as well as the number of reactants are fixed and we do not consider the DFT system to be open to these species. We therefore require that only the chemical potentials of ions are fixed by the bulk solution and that the chemical potential of electrons is fixed by the electrode. These constraints lead to a *partial grand canonical DFT* in terms of the ions and electrons with fixed chemical potentials.

Before advancing further, it needs to be noted that the particle number operators of the nuclear degrees of freedom correspond to only nuclei, not electrons attached to it forming an ion. Still, one can simplify the treatment of the nuclear chemical potentials as only a mean ion chemical potential is needed. This is because experimentally the concentration of ions in the bulk solution needs to respect electroneutrality, and thus, the concentration of a nucleus corresponding to an ion cannot be changed independently.[40] Due to this restriction, chemical potentials in two phases (here the bulk b and interface η) are bound by the constraint for cationic nuclei (+) and anionic nuclei (−). For a binary electrolyte, it holds that

$$\tilde{\mu}_\pm^b = v_-\tilde{\mu}_-^b + v_+\tilde{\mu}_+^b = v_+\tilde{\mu}_+^\eta + v_+\tilde{\mu}_-^\eta = \tilde{\mu}_\pm^\eta, \qquad (4)$$

where v_i is the stoichiometric coefficient and $\tilde{\mu}_i = \mu_i^0 + q_i\phi(\mathbf{r})$ with q_i as the charge and $\phi(\mathbf{r})$ as the Galvani (inner) potential. ϕ of the two phases are different, leading to an imbalance in concentrations between different phases. In the liquid phase, we can take $\phi^b = 0$ as will be discussed in Sec. II E. Following Guggenheim,[40] the mean activity coefficient for η phase is $\gamma_\pm^{v_+ + v_-} = \gamma_+^{v_+}\gamma_-^{v_-} = \gamma_\pm^\alpha$ for phase α. The mean absolute activity is defined in terms of the concentration c and standard chemical potential $\mu^0 = \beta \ln \lambda^0$ where λ^0 depends on the solvent, temperature, ions, etc. (later it will be realized that λ^0 is related to the thermal de Broglie wavelength). The chemical potential of nuclei for the ions forming the electrolyte is

$$\tilde{\mu}_\pm^\eta = \beta^{-1} \ln[\gamma_\pm^\eta (\lambda_\pm^0)^{v_+ + v_-} (c_-^\eta)^{v_-} (c_+^\eta)^{v_+}] = \mu_\pm^b. \qquad (5)$$

For this reason, the relevant chemical potential of the ionic nuclei forming the electrolyte is the bulk chemical potential $\mu_\pm^b = \mu_\pm^N$ where N reminds that at the point, the ionic chemical potential is only for the nuclei of the ions, not ions with a nucleus and electrons related to a specific nucleus. The grand canonical free energy for an electrochemical system with fixed ionic nuclear (±) and electron (n) chemical potentials is

$$\Omega(T, V, \tilde{\mu}_\pm^N, \tilde{\mu}_n) = \text{Tr}[\hat{\rho}\hat{\Omega}] \equiv \Omega[\hat{\rho}]$$

$$= \sum_i p_i^{GC}\Bigg[Tk_b \ln p_i^{GC} + \Big\langle\Psi_i|\hat{H}_{tot}$$

$$- \mu_\pm^N(\hat{N}_+ + \hat{N}_-) - \tilde{\mu}_n\hat{N}_n |\Psi_i\Big\rangle\Bigg], \qquad (6)$$

where $Tk_b p_i \ln p_i = -TS$ as $p_i \ln p_i = -S$ is the von Neumann entropy.[41]

Now we turn to the minimization of the partial grand canonical energy. This is performed following Levy's constrained search[11,42] with the grand canonical Hamiltonian. To specify the external potential in a chemically meaningful way and for future convenience, we split the total nuclear density from all the nuclei N in the system to well defined contributions of nuclei comprising the solvent S, nuclei of ions in the solution I, nuclei in the electrode M, and nuclei of possible reactants R. Similarly, the total electron density n can be split into contributions from the electrolyte ions $n_\pm(\mathbf{r})$, electrode

$n_e(\mathbf{r})$, and solvent molecules $n_s(\mathbf{r})$. Furthermore, the positions of the atoms constituting the electrode and the reactants are fixed and considered explicitly. Thus, we choose that the external potential $v(\mathbf{r})$ is defined by the electrode and reactant nuclei and given by

$$v(\mathbf{r}) = \sum_a^{M,R} \int d\mathbf{r}' \frac{\rho_a(\mathbf{r}')}{|\mathbf{r} - \mathbf{r}'|} \approx \sum_a^{M,R} \frac{Z_a(\mathbf{R}_a)}{|\mathbf{r} - \mathbf{R}_a|}. \tag{7}$$

The first definition corresponds to an effective nuclear potential due to a quantum nucleus a which is approximated by the classical point like nuclei having the charge Z_a. By specifying the external potential this way, the corresponding quantity needs to be removed from $\hat{H}_{tot}$. By this choice, part of the system is to be considered fixed providing a static external potential to the electrons and rest of the nuclei. This is reminiscent of a Born-Huang (BH) approximation for fixed nuclei with positions $\bar{\mathbf{R}}_{M,R}$ [in the absence of non-adiabatic effects, the Born-Oppenheimer (BO) approximation is sufficient]. Thus, the total wave function is approximated as a product of the fixed (not yet classical) nuclei of the reactants/electrode and the mixed wave function of ionic nuclei, solvent nuclei, and the electrons of the entire system,

$$\hat{\rho} = \sum_i p_i \sum_{kj} |\psi_{ij}(\mathbf{r}_n, \mathbf{R}_{I,S}; \bar{\mathbf{R}}_{M,R}) \Phi_j(\bar{\mathbf{R}}_{M,R})\rangle$$
$$\times \langle\psi_{ik}(\mathbf{r}_n, \mathbf{R}_{I,S}; \bar{\mathbf{R}}_{M,R}) \Phi_k(\bar{\mathbf{R}}_{M,R})|,$$

with

$$|\Psi_i\rangle = \sum_j |\psi_{ij}(\mathbf{r}_n, \mathbf{R}_{I,S}; \bar{\mathbf{R}}_{M,R}) \Phi_j(\bar{\mathbf{R}}_{M,R})\rangle, \tag{8}$$

where the nuclear-electronic wave functions are written using the BH expansion to factor the wave function with Φ as the nuclear wave function for the reactants/electrode and ψ for the combined electronic and solvent/ion nuclear wave function. As a result, the electrons and solvent/ion nuclei move on the potential energy surface generated by the nuclei of the electrode and reactants. While the BH separation has been assumed, the adiabatic theorem (see, for example, Sec. 5.1 in Ref. 43) has not been invoked and therefore nonadiabatic effects are still present. Finally, either diabatic or adiabatic ion/electron wave function can be utilized in the above expansion; the latter is more suitable for general chemical reactions, while the former may prove to be convenient for the study of electron and proton transfer reactions, for example.

To further simplify the situation, the nuclei of the electrode and reactant are assumed classical. Such a division is obtained by splitting the total partition function as a restricted partition function $\bar{\Xi}$[44] with fixed classical nuclei with momentum $\bar{\mathbf{P}}$ and subsequently sampling the phase space of the classical nuclei. Thus, the total quantum grand canonical ensemble is approximated as a system where the open quantum system interacts with the fixed, classical nuclei. For this system, the grand partition function is

$$\Xi(T, V, \tilde{\mu}_\pm, \tilde{\mu}_n) \approx \frac{1}{N_M! N_R! h^{3(N_M + N_R)}} \int d\bar{\mathbf{R}}_{M,R} d\bar{\mathbf{P}}_{M,R} \exp\left[-\beta \sum_N^{M,R} \frac{\bar{\mathbf{P}}_N^2}{2M_N}\right] \bar{\Xi}(T, V, \mu_\pm^N, \tilde{\mu}_n; N_M, N_R, \bar{\mathbf{R}}_{M,R})$$

$$= \frac{1}{N_M! N_R! \lambda^{3(N_M + N_R)}} \int d\bar{\mathbf{R}}_{M,R} \exp\left[-\beta \Omega(T, V, \mu_\pm^N, \tilde{\mu}_n; N_M, N_R, \bar{\mathbf{R}}_{M,R})\right]$$

$$= \frac{1}{N_M! N_R! \lambda^{3(N_M + N_R)}} \int d\bar{\mathbf{R}}_{M,R} \exp\left[-\beta \text{Tr}\left[\hat{\rho}\left(\hat{H}_{tot} - \hat{T}_N^{M,R} + T k_b \ln[\hat{\rho}] - \sum_j \tilde{\mu}_j \hat{N}_j\right)\right]\right]$$

$$= \frac{1}{N_M! N_R! \lambda^{3(N_M + N_R)}} \int d\bar{\mathbf{R}}_{M,R} \exp\left[-\beta \text{Tr}[\hat{\rho}\hat{\Omega}_{BH}]\right], \tag{9}$$

where the quantum mechanical nuclear kinetic energy has been replaced by its classical equivalent and λ is the thermal de Broglie wavelength unique for a given nuclear type. The grand free energy from above is for classical nuclei of the electrode and reactants interacting with the quantum system of electrons, solvent, and ionic nuclei. The classical mechanics for reactant and electrode nuclei is implied by the use of a classical partition function for these degrees

of freedom. The free energy contributions from the classical part can be obtained by thermal sampling of the R, M degrees of freedom, while free energy of the quantum part is obtained directly from density functional theory. It is also worth noting that electronic nonadiabatic effects are still included and can be computed schemes from mixed quantum-classical dynamics,[45] but then one does not integrate out the momenta.

The formal quantum/classical separation leads to an external potential which is defined by the last quantity in Eq. (7). If some nuclei of the reactants or electrode need to be treated quantum mechanically (e.g., in tunneling calculations), these selected nuclei can be modeled using the nuclear-electron orbital DFT (NEO-DFT),[46] for example. Also the zero point energies for the reactant and electrode nuclei can be approximated by, e.g., solving the nuclear wave functions on the GC-BH potential energy surface. After the BH separation with fixed classical nuclei, the minimum grand canonical energy for the quantum system of electrons, ions, and the solvent reads

$$\Omega(T, V, \mu_\pm^N, \tilde{\mu}_n; N_M, N_R, \bar{\mathbf{R}}_{M,R}) = \mathrm{Tr}[\hat{\bar{\rho}}\hat{\Omega}_{BH}]$$

$$= \min_{n(\mathbf{r}), \{N_{I,S}(\mathbf{R})\}} \left\{ F^\tau[n(\mathbf{r}), \{N_{I,S}(\mathbf{R})\}] + \int d\mathbf{r} \left[v(\mathbf{r}) \left(\sum_a^{M,R,I,S} N_a(\mathbf{r}) - n(\mathbf{r}) \right) - \tilde{\mu}_n n(\mathbf{r}) - \sum_i^I \mu_i^N Z_i(\mathbf{r}) \right] \right\}, \quad (10)$$

where

$$F^\tau[n(\mathbf{r}), \{N_{I,S}(\mathbf{R})\}] \equiv \min_{\hat{\bar{\rho}} \to [n(\mathbf{r}), \{N_{I,S}(\mathbf{R})\}]} \mathrm{Tr}[\hat{\bar{\rho}}(\hat{\Omega}_{BH} - \hat{v}(\mathbf{r}))]. \quad (11)$$

The above yields the exact grand canonical energy for a grand canonically treated quantum subsystem interacting with classical nuclei setting the external potential. Together Eqs. (9) and (10) form the general GC-DFT expression for electrochemical systems at fixed electron and ion chemical potentials.

B. Classical/electronic GC-DFT for electrocatalytic systems: Joint GC-DFT

Of course the exact functional in Eq. (11) is highly complex and needs further simplification. In order to simplify the functional, we assume that also the ion and solvent nuclei are classical. Then, we seek to combine the electronic system using quantum mechanical DFT with a classical description of the electrolyte, both with fixed chemical potentials. In the canonical ensemble, this is achieved using joint DFT[12,25] (for convenience, the canonical JDFT is presented in the supplementary material). While the canonical JDFT approach offers a fully DFT way of computing Helmholtz canonical free energies, typical systems treated within (electronic) DFT are very small due to the computational burden of such calculations and fluctuations in the chemical potentials may occur during, e.g., reactions. Therefore, we seek a fixed potential version of canonical JDFT and derive a general GC-JDFT starting from the multi-component GC-DFT presented in Sec. II A.

Computational methods based on classical DFT use classical force-fields for describing both inter- and intra-molecular interactions (see, e.g., Ref. 47). One specific aspect of the classical force field models is the assignment of partial charges to atoms in order to simulate electrostatic interactions. While polarization can be included, the partial charges typically remain unchanged and are spatially invariant. Partition of charges is conceptually and practically inconvenient in

the view of the above DFT formulation; according to Eq. (10), the electrons are completely smeared throughout the entire system and the electron chemical potential acts on all electrons. Thus, the total electron density needs to be separated to "quantum" and "classical" contributions.

Such a separation is closely related to the partial charge transfer at the electrochemical interface.[48] The charge state of an ion or a solvent molecule at the interface can differ from its bulk value. The charge transfer is indicative of covalent bonding or specific adsorption both of which warrant a quantum mechanical description.[48] Charge transfer is not confined to only adsorbed species but can take place also in the outer Helmholtz layer.[49] While a fully quantum mechanical treatment naturally includes the covalent bonding and charge transfer, including such phenomena in classical DFT and thermodynamics needs extrathermodynamic or modelistic assumptions regarding how the total charge of the interface is partitioned between the metal and the liquid electrolyte.[48,50]

The above considerations call for a formal way to identify how changing concentration or particle number at a specific position changes the energy. Such spatially resolved energy dependence can be achieved by introducing a position dependent chemical potential which measures how a change in the local concentration $c_i(\mathbf{r})$ changes the grand energy. A position dependent chemical potential also allows defining regions with different electrophilicity or ionophilicity.[51] Accordingly, the position dependent chemical potential density is

$$\tilde{\mu}_i(\mathbf{r}) = \left(\frac{\delta A}{\delta N_i(\mathbf{r})} \right)\Bigg|_{v(\mathbf{r}),T}, \quad (12)$$

with $\int_V d\mathbf{r}\mu_i(\mathbf{r}) = \mu_i$. Here the integration volume V is a point in a solvent volume for continuum ion models such as the Poisson-Boltzmann model, the effective ion volume in explicit particle simulations, or the electrons at the electrode surface in contact with the bulk, for example. By integrating the chemical potential density over the effective volume, one obtains a constant chemical potential for the species everywhere, and thus, thermochemical equilibrium is maintained.[52] However,

the choice of the effective volume introduces an additional assumption as in the quantum system, only the electron and nuclear chemical potentials are specified; partitioning of the chemical potential in order to identify species is based on chemical or physical intuition. A specific case for the ions is further clarified below.

Such a formal definition allows local partition of the nuclear and electronic densities to chemically meaningful quantities such as molecules as performed in molecular grand-canonical ensemble theory.[53] We utilize the spatial dependence of the chemical potential density to partition the total electron density to electrons at the electrode and ions with a specified charge confined in the solution. To allow the electrochemical potential of electrons to be treated independently of the ion chemical potential, the electron density is partitioned to well defined contributions from the electrode and reactants as well as from the ions and solvent. This separation is achieved by splitting the total nuclear and electronic densities to the electrode/reactant and ion/solvent contributions. We also demand that the partitioned densities sum up to the densities as performed in subsystem DFT:[54] $n(\mathbf{r}) = n_\pm(\mathbf{r}) + n_e(\mathbf{r}) + n_s(\mathbf{r})$ and $N_E(\mathbf{r}) = N_R(\mathbf{r}) + N_M(\mathbf{r}) + N_I(\mathbf{r}) + N_S(\mathbf{r})$.

The GC free energy in the presence of charge transfer is naturally obtained from minimization of Eq. (10). If we are to exclude charge transfer between the M, R and N, I subsystems, the grand energy is also altered. Making the constituents of N, I subsystem bear the same charge as they do in the bulk phase means that we are changing the molecular nature of these species. The GC free energy change for such process is written as[53]

$$dΩ = dE - \int_V d\mathbf{r}[\mu_n(\mathbf{r})dn(\mathbf{r}) + n(\mathbf{r})d\mu_n(\mathbf{r}))]$$
$$- \int_V d\mathbf{r}[\mu_\pm^N(\mathbf{r})dN_I(\mathbf{r}) + N_I(\mathbf{r})d\mu_\pm^N(\mathbf{r}))]. \quad (13)$$

We are interested only in the case where the chemical potentials stay fixed and allow the number of species. Because the chemical potential densities are spatially defined, we can confine them to specific regions. We use this freedom to partition the total volume to quantum V_q (comprising of the electrode and reactants) and classical V_c volumes (comprising of the ions and solvent). While this not necessary, the partition to "quantum" and "classical" regions reflects the choice of treating the electrons from the electrode and reactants as quantum mechanically and ions/solvent classically with confined electron densities and helps if the two subsystems are to be treated separately. Also with this choice, one can define an ion chemical potential $\mu_\pm$ which corresponds to electrons and ionic nuclei bound together. Ionic nuclei and electrons in equilibrium form an ion with a specific charge Z_+ or Z_- for cations and anions, respectively. In particular, for the chemical potential of cations μ_+ in equilibrium we have

$$\mu_n(\mathbf{r}) + \mu_+^N(\mathbf{r}) = \mu_+(\mathbf{r}) \quad (14)$$

such that $\int_{V_{ion}} d\mathbf{r}(\mu_n(\mathbf{r}) + \mu_+^N(\mathbf{r})) = \int_{V_{ion}} d\mathbf{r}\mu_+(\mathbf{r}) = \mu_+$ and $\int_{V_{ion}} d\mathbf{r}(n(\mathbf{r}) + N_+(\mathbf{r})) = \int_{V_{ion}} d\mathbf{r}\rho_+(\mathbf{r}) = Z_+$. This allows one to specify ions with a well-defined charge. A similar splitting can be performed for the solvent molecules as well. Note that we have chosen the effective volume of a species in order to obtain the charges of ions/solvent based on chemical intuition. Per this choice, the integration volume/shape depends spatially on the chemical potential density related to our choice of an "ion." This choice also changes the GC free energy according to Eq. (13), and the GC-JDFT energy will differ from the GC-MCDFT energy.

Finally, we introduce the split densities and volumes with the spatial chemical potential densities in Eq. (10) and obtain

$$Ω(T, V, \mu_\pm, \tilde{\mu}_n; N_M, N_R, \bar{\mathbf{R}}_{R,M}) \approx \min_{n(\mathbf{r}), \{N_{I,S}(\mathbf{r})\}} \left\{ F^\tau[n(\mathbf{r}), \{N_{I,S}(\mathbf{R})\}] + \int_{V_q} d\mathbf{r}\left[v(\mathbf{r})\left(\sum_a^{M,R} Z_a(\mathbf{r}) - n_e(\mathbf{r})\right) - \tilde{\mu}_n n_e(\mathbf{r})\right] \right.$$
$$\left. + \int_{V_c} d\mathbf{r}\left[(v(\mathbf{r}) - \mu_\pm)\rho_\pm(\mathbf{r}) + v(\mathbf{r})\left(\sum_S Z_S(\mathbf{r}) - n_s(\mathbf{r})\right)\right]\right\}, \quad (15)$$

with the ionic charge density $\rho_\pm(\mathbf{r})$.

The chemical potential density enables us to separate classical species and regions from the quantum mechanical system and specify charges of different species and subsystems. Then, taking inspiration from the JDFT approach,[12] the electron density due to the solvent and ions can be integrated out,

$$Ω(T, V, \mu_\pm, \tilde{\mu}_n; N_M, N_R, \bar{\mathbf{R}}) = \min_{n(\mathbf{r}), \{N_{I,S}(\mathbf{r})\}} \left\{ G^\tau[n(\mathbf{r}), N_{I,S}(\mathbf{r})] + \int_{V_q} d\mathbf{r}\left[v(\mathbf{r})\sum_{a\in M+R} Z_a(\mathbf{r}) + (v(\mathbf{r}) - \tilde{\mu}_n)n(\mathbf{r})\right] \right.$$
$$\left. \times \int_{V_c} d\mathbf{r}[(v(\mathbf{r}) - \mu_\pm)\rho_\pm(\mathbf{r}) + v(\mathbf{r})\rho_S(r)]\right\}, \quad (16)$$

where the solvent charge density ρ_S has been introduced and

$$G^\tau \equiv \min_{n_\pm(\mathbf{r}), n_s(\mathbf{r})} \left[F^\tau[n, \{N_{I,S}\}] + \int d\mathbf{r} v(\mathbf{r}) \left(\sum_a^S Z_a(\mathbf{r}) - n_s(\mathbf{r}) \right) + \int d\mathbf{r} v(\mathbf{r}) \left(\sum_a^I Z_a(\mathbf{r}) - n_i(\mathbf{r}) \right) \right]. \quad (17)$$

The last two equations yield the grand free energy of a microscopic electrode-electrolyte interface where the ion and electron chemical potentials can be explicitly controlled independently and where the solvent and ions have well-defined charges needed for classical simulations of the electrolyte.

The goal of the minimization was to obtain separation of electrons belonging to the electrode and the electrolyte in order to manipulate the electrode potential and ion chemical potentials separately. Furthermore, the solvent and ions were constructed so that the ion and solvent molecules have well-defined charges. Care was also taken to partition the constraints due to chemical potentials in chemically meaningful entities.

It is important to stress that integrating out the solvent and ion electrons prevents exchange of electrons between the solvent/ions with the electrode/reactants and prevents the formation of a covalent bond between the ions/solvent with the quantum region; only electrostatic, polarization, and dispersion-like interactions can be captured with the presented partitioning. Also, the enforced constraint that all species have the same charge independent of the position excludes all charge transfer effects. Note that a similar situation is encountered whenever effective (atomic) charges are predefined for ions or solvent molecules. Prominent examples of such are classical DFT within the RISM approach[15] discussed below and detailed in the supporting information of Ref. [15] or in the force fields used in classical molecular dynamics simulations. This has direct implications on the applicability mixed classical/quantum systems. In the current setting, the most important restriction is that specific adsorption of the solvent/ions cannot be captured with confidence.

C. Classical continuum/electronic GC-DFT for electrocatalytic systems

The next (still formidable) challenge is to find the free energy functionals for the quantum subsystem, classical electrolyte, and their interactions. While the quantum part is available from electronic DFT, the electrolyte density can be obtained from the classical theories such as classical DFT.[7] Currently, the most sophisticated approaches combine electronic DFT with RISM.[13–15] The combination of DFT and RISM yields a highly complicated set of coupled equations to be solved self-consistently. Yet, even in the DFT-RISM approach, the solvent and ions are treated using "equilibrium classical statistical mechanics applied to thermodynamics of surface phenomena. Quantum

mechanical approaches to surface phenomena are excluded. . .. Therefore, all aspects related to chemisorption and catalytic processes at surfaces are not considered" as discussed on p. 883 of Ref. [55]. In the current setting specifically adsorbed species forming covalent bonds or exchanging charge with the surface need to be treated as reactant, as discussed in Sec. II B.[15,33]

To obtain a computationally feasible method, we simplify the situation, and for a moment, consider the electrode and electrolyte interacting only via a static field created by the other component. The setup is similar (but simpler) to frozen-density embedding where one system is kept frozen, while the other one is relaxed in the field of the frozen subsystem. In the simplest case, the electrolyte will feel electrostatic potential set by the electrons and nuclei in the electrode. Within the classical GC-DFT framework, the free energy of the electrolyte is written as[56]

$$\Omega(\{\rho_i\}) = \sum_i \int_{V_c} d\mathbf{r} \rho_i(\mathbf{r}) (V_{ext}(\mathbf{r}) - \mu_i)$$
$$+ \beta^{-1} \sum_i \int_{V_c} d\mathbf{r} \rho_i(\mathbf{r})[\ln(\lambda^3 \rho_i(\mathbf{r})) - 1] - F_{ex}[\{\rho\}], \quad (18)$$

where V_{ext} is the external potential due to ions, solvent as well as a genuine external potential (in our case from the quantum subsystem) and λ is the thermal de Broglie wavelength. The first term accounts for the Coulomb interactions of the pure component, the second is the ideal gas entropy, while F_{ex} accounts for excess free energy due to additional interparticle interactions. Also note that F_{ex} is a universal functional of the classical densities.

We adopt the classical DFT and further assume that the solvent can be treated as a (non-homogeneous) dielectric. At this level of theory, the dielectric presents how the liquid responds to an electric field. In general, this response is a non-local and non-linear function.[57,58] The general response between displacement field (D) is connected to the electric field and polarization by $D = E + 4\pi P$. If the polarization depends linearly on the electric field, one obtains $D(\mathbf{r}) = \epsilon(\mathbf{r})E(\mathbf{r})$, where $\epsilon(\mathbf{r})$ is the dielectric function. At interfaces, the dielectric function is a tensorial quantity as perpendicular and parallel contributions as polarization depends on the direction. Both components can exhibit complex, non-monotonous behavior reflecting the interaction between the surface and the solvent.[58]

The dielectric approximation to classical DFT can be obtained by following Sluckin.[9] In this situation, the free energy of the electrolyte can be written as

$$\Omega_i = \int_{V_c} d\mathbf{r} \rho_\pm(\mathbf{r})(\phi(\mathbf{r}) - \mu_\pm) - \frac{1}{8\pi} \int_{V_c} d\mathbf{r} \epsilon(\mathbf{r}) |\nabla \phi(\mathbf{r})|^2$$
$$+ \beta^{-1} \sum_i \int_{V_c} d\mathbf{r} \rho_i(\mathbf{r})[\ln(\lambda^3 \rho_i(\mathbf{r})) - 1] + F_{ex}[\{\rho\}], \tag{19}$$

where $\phi = V_{ext}(\mathbf{r}) + V_{ions}$ is the effective electrostatic due to the external potential $V_{ext}(\mathbf{r})$ induced by the charge density of the electrode and charge density of the ionic distribution V_{ions}. Presented in this form, it would be possible to sample the ionic distribution in a dielectric solvent in the presence of an external potential formed by the electrode. We will, however, look for the minimum of the free energy functional. This is effectively the derivation of the Poisson-Boltzmann equation which fixes the chemical potential of the ions combined with the grand canonical electronic DFT developed by Mermin.[10] Similar derivations have been performed before in the literature, and the interested reader may found our derivation in the supplementary material,

$$\Omega[T,V,\tilde{\mu}_n,\mu_\pm] = \min_{n,\rho_\pm} \left[\min_{\hat{\rho} \to n, \rho_\pm} \left(A_{KSM}[n] - \frac{1}{8\pi} \int d\mathbf{r} \epsilon(\mathbf{r}) |\nabla \phi(\mathbf{r})|^2 \right. \right.$$
$$\left. + G(n(\mathbf{r}), \rho_\pm(\mathbf{r})) \right) + \int d\mathbf{r}(\phi(\mathbf{r}) - \tilde{\mu}_n)n(\mathbf{r})$$
$$\left. + \int d\mathbf{r}(\phi(\mathbf{r}) - \mu_\pm)\rho_\pm(\mathbf{r}) \right]. \tag{20}$$

An important difference compared to usual mPB models is that electrocatalytic systems are usually partly periodic. Since we are not allowing the number of nuclei or electrons from the solvent, nuclei from the electrode, or reactant to fluctuate, electroneutrality sets a constraint that the electron density from the quantum system must always be compensated by the ionic charge density: $\int_{V_q} d\mathbf{r}(\sum_{a \in M,R} Z_a(\mathbf{r}) - n(\mathbf{r})) = \int_{V_c} d\mathbf{r}\rho_\pm(\mathbf{r})$. This aspect is extensively discussed in Sec. II F below. To arrive at the equation above, we have invoked the BO and adiabatic approximations and terms coupling the nuclear motion to the electronic density have been removed and the equation is a modified Kohn-Sham-Mermin (KSM) embedded in the dielectric environment with continuum ions.

D. Generalized Poisson-Boltzmann equation for the electric double-layer: Including Stern layer and ionic hydration

The GC-DFT approach introduced in Sec. II C puts implicit solvent models on a firm theoretical basis. The generalized Poisson equation and the derived potential are the working equations in the common implicit solvation models, such as the one implemented in GPAW.[59] However, electrochemical systems add yet another layer of complexity since the solvent contains mobile ions which form a double-layer at the electrochemical interface.

To include the electrolyte and the double-layer, an ionic density is added to the generalized Poisson equation.[25,30] To obtain a self-consistent scheme for the inclusion of the solvation effects, Eq. (20) needs to be minimized with respect

to ϕ and then with respect to the solute electron density $n(\mathbf{r})$ as well as the ionic density. Before carrying out the minimization, we need to decide which interactions to include in the model. While the non-linear polarization of the fluid can be important for treating electrochemical interfaces,[37] we assume as a first approximation that the polarization response of the fluid to the electrostatic potential is linear and consider only a linear dielectric. However, we consider several non-linear and ion-specific interactions in the ion free energy:

1. It has been shown in Refs. 60 and 61 that dielectric decrement due to ion solvation leads to salt-specific interactions and improves the description of the double-layer in classical simulations. The simplest way to include the solvated ion effects is a linear dependence between the dielectric constant and the ion density,

$$\epsilon[c_\pm(\mathbf{r})] = \epsilon_0 - \alpha_\pm c_\pm(\mathbf{r}), \tag{21}$$

where ϵ_0 is the dielectric constant of the pure solvent and $\alpha_\pm$ is an ion specific parameter which is available for a range of ions. The model also changes the dielectric constant of the bulk solution as observed for several simple electrolytes (see Ref. 62 and references therein). The ionic concentrations c_i and charges q are related to ionic charge densities via

$$\rho_\pm(\mathbf{r}) = \sum_i q z_i c_i(\mathbf{r}). \tag{22}$$

2. Mean field chemical interactions between the electrolyte and quantum system need to be included. These interactions between the solvent and the quantum subsystem include cavitation, dispersion, and (Pauli) repulsion in the following form:[35]

$$G_{chem} = \gamma \int d\mathbf{r} |\nabla S(\mathbf{r})|, \tag{23}$$

where ∇S is the solvent accessible area of the quantum system and γ is an effective surface tension term to be fitted to experiments.

3. Finite size of the ions is included to account for steric effects and avoid unphysically large ion concentrations near the electrode surface which can also be seen as formation of the Stern layer due to specific adsorption. These are entropic effects due to charge organization and can be accounted for using the Bikerman-Freise approach[63] (also often cited as Borukhov's method[64]),

$$-TS_{ions} = \frac{\beta^{-1}}{a^3} \int d\mathbf{r} c_\pm(\mathbf{r})a^3 \ln(c_\pm(\mathbf{r})a^3)$$
$$+ (1 - c_\pm(\mathbf{r})a^3)\ln(1 - c_\pm(\mathbf{r})a^3), \tag{24}$$

where it is assumed that all ions have the same effective size a^3.

4. In recent studies,[29,37] electronic DFT has been combined with mPB which includes a separate Stern exclusion layer. This simple approach has been shown to lead

to improved description differential capacitance,[37] radial distribution functions, and free energy of solvation in electrolytes.[29] The exclusion width is linked to the ion hydration number[29] and therefore its size a.

These effects are included either in the dielectric constant or in the free energy in Eq. (20). The additional free energy is written as $G[n(\mathbf{r}), \rho_\pm] = G_{chem} - TS_{ions}$. Under these assumptions, the minimization of Eq. (20) with respect to the ionic concentration under the boundary conditions $c_\pm(bulk) = c_b$ and $\phi(bulk) = 0$ (see also the discussion in Sec. II E related to the boundary conditions) gives the ionic distributions as[60,61]

$$c_\pm(\mathbf{r}) = \frac{\mathcal{C}_\pm(\mathbf{r})}{1 + 2c_b a^3 + a_\pm^3 (\mathcal{C}_+(\mathbf{r}) + \mathcal{C}_-(\mathbf{r}))}, \tag{25a}$$

$$\mathcal{C}_\pm(\mathbf{r}) = c_b \exp\left[\mp \beta z e \phi + \frac{\beta \partial \epsilon}{8\pi \partial \rho_\pm} |\nabla \phi|^2 \right], \tag{25b}$$

and $c_b = \exp[\beta^{-1} \mu_\pm]/a^3$. Note that the last quantity of Eq. (25b) is the dielectric decrement which is related to the water dipole rearrangement in the Kralj-Iglic model,[65] in a microfield model Garish and Promislow,[62] and in Booth's[66] dielectric model where the water dipole orientation is proportional to $\sim \exp[\nabla \phi]$. The ion decrement affects both the bulk dielectric constant and the double layer where the (counter) ion concentration is high.

Because additional "chemical terms" are independent of electron density, minimization of Eq. (20) against the electron density leads to the KSM equation presented in Eq. (13) in the supplementary material. The only modification to this equation is that in practice, no separate Hartree, external, or electrostatic potential terms are needed as the total electrostatic potential is obtained from the Poisson-Boltzmann equation resulting from the minimization of (20) against the total charge density,

$$\nabla[\epsilon(\mathbf{r}) \nabla \phi(\mathbf{r})] = -4\pi[-N(\mathbf{r}) + n(\mathbf{r}) + \rho_\pm(\mathbf{r})], \tag{26}$$

where $\rho_\pm[\phi](\mathbf{r})$ is the spatial density of concentration of ions in the dielectric given by Eq. (22). Finally, the free energy and effective potential for the coupled KSM-electrolyte system are obtained after a partial integration of the electrostatic terms

$$\Omega = -\frac{1}{2} \sum_i \langle \psi_i | \nabla^2 | \psi_i \rangle - \int d\mathbf{r} v_{xc}(\mathbf{r}) n(\mathbf{r})$$
$$+ \frac{1}{2} \int d\mathbf{r} \phi(\mathbf{r}) [n(\mathbf{r}) + \rho_\pm(\mathbf{r}) - N(\mathbf{r})] - \int d\mathbf{r} \tilde{\mu}_n n(\mathbf{r})$$
$$- \int d\mathbf{r} \mu_\pm \rho_\pm(\mathbf{r}) - TS_{ions} + G_{chem}, \tag{27a}$$

$$V_{eff,\Omega}(\mathbf{r}) = v_{xc}(\mathbf{r}) + \frac{1}{2}\phi(\mathbf{r}) - \frac{\partial \epsilon(\mathbf{r})}{8\pi \partial n(\mathbf{r})} |\nabla \phi(\mathbf{r})|^2 - \tilde{\mu}_n, \tag{27b}$$

where the electron and ion densities are given by the equation for electron density in grand canonical ensemble

[supplementary material, Eq. (14)] and (22), respectively. The above set of equations offers a feasible approach to include the electrolyte and the presence of a double-layer in the simulations. From a computational point of view, inclusion of the ionic density can also simplify the treatment of charged periodic systems; in the best case scenario, the electrolyte neutralizes the simulation cell and the use of artificial background charge can be avoided. However, the absolute neutralization is achieved automatically for linear PB models.[32] For other mPB models, the charge neutrality needs to be enforced as discussed in detail in Sec. II F. Coupling mPB with Fermi-level control from electronic GC-DFT provides powerful machinery for modeling electrocatalytic reactions at electrochemical interfaces under constant electrode and ionic potentials.

E. Electrode potential

Upon deriving the Poisson-Boltzmann distributed ion concentration, a boundary condition for electrostatic potential was chosen as to approach zero in the bulk liquid phase. This provides a very convenient reference electrode corresponding to electrons solvated in the electrolyte. To appreciate this, one can consider the definition of the absolute electrode potential by Trasatti,[67]

$$E^M(abs) = E^M(red) + K, \tag{28}$$

where K is a constant depending on the absolute reference choice and $E^M(red)$ is the reduced absolute potential,

$$E^M(red) = \Delta \phi_S^M - \mu_n^M, \tag{29}$$

where $\Delta \phi_S^M$ is the Galvani, i.e., electric potential difference between the electrode and bulk liquid and μ_n^M is the chemical potential of electrons, i.e., the Fermi-level. One possible choice for the reference K is an electron interacting electrically but not chemically with the environment corresponding to $K = \mu_n^S$.[68] While this choice for the reference cannot be realized experimentally, this is exactly produced by the PB-model *for a given model electrolyte and choice of PB boundary conditions*.

Making the approach even more transparent, we consider the electrode potential under equilibrium conditions using the solvated electron reference which yields

$$E(abs)^{PB} = \tilde{\mu}_n^S - \tilde{\mu}_n^M = \mu_n^S - \mu_n^M - (\phi^S - \phi^M)$$
$$= -\mu_n^M + \phi^M = -\tilde{\mu}_n^M, \tag{30}$$

where $\tilde{\mu}_n^i$ is the electrochemical potential of electrons in phase i. From the above choice of PB-boundary conditions, we know that $\phi^S \to 0$ in the fluid and that PB-model accounts only for the electrostatic interactions from which $\tilde{\mu}_n^S = 0$ follows. Therefore the absolute electrode potential within the PB-solvation model is given in the two right-most form of Eq. (30), i.e., the Fermi-energy E_F. A similar conclusion was made earlier[25] for the linearized Poisson-Boltzmann mode, but as shown, the $\phi^S \to 0$ is obtained from the correct choice of boundary conditions

and can be used for all mPB models, the effective screening method (ESM) method by Otani and Sugino,[16] or the modified boundary condition method of the present work (see Sec. II F 2 and the supplementary material).

In practice, the absolute electrode potential needs to be presented on an experimentally relevant reference scale, e.g., against the standard hydrogen electrode (SHE). While $\tilde{\mu}_n^S = 0$ in the PB-model, this choice depends on the actual implicit solvation model used for the electrolyte, and therefore, a connection between the model fluid and an experimental reference electrode needs to established. While several alternatives exist for the absolute potential,[68] the most viable reference is an electron at rest in vacuum close to the surface of the solution–this absolute potential of SHE varies between 4.2 and 4.8 V. One therefore needs to convert $E(abs)^M$ from the PB-solvent reference to this vacuum reference. For this, we refer again to the absolute potentials by Trasatti[67] and all relevant quantities are summarized in Fig. 2.

A practical way to connect the PB fluid with a real solvent compute the potential of zero charge (PZC) using PB and compare it to experimental results for the same electrode and the same electrolyte. Formally, this is obtained by equating the absolute PZCs of the electrodes in the PB-solvent with the solvent reference and real electrolyte with a vacuum reference; the constant off-set could, in principle, be obtained from

$$\Delta \chi_S = \chi_S^{PB} - \chi_S = E_{PZC}^{PB}(abs) - E_{PZC}(abs), \tag{31}$$

which is highly dependent on the implementation and calculation details.[69] This off-set can be used to convert the PB-scale to SHE-scale by

$$\Delta E(SHE) = E^{PB}(abs) - \Delta \chi_S - E^{SHE}(abs), \tag{32}$$

which, in practice, requires knowing the PZC against the absolute SHE.

Another plausible approach which directly gives the $E(abs)^{PB}$ referenced directly against the vacuum reference[67,68] was introduced and applied by Otani.[70] Here an asymmetric surface with vacuum on the other and solvent on the other side can be used to compute contact (Volta) potentials of both the electrode and solvent as well as the surface potentials. These could be used to convert the PB-solvent reference to a vacuum reference without any experimental input on PZC, but in practice, some experimental data are needed.
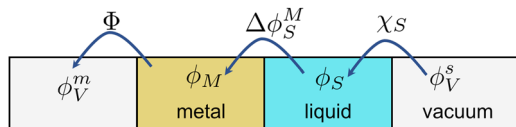
FIG. 2. Schematic of inner potential ϕ_M, outer potential ϕ_S, surface potential χ_S, work function Φ, vacuum potential on the solvent side ϕ_V^s, and vacuum potential on the metal side ϕ_V^s.

F. Charge neutrality within continuum models

When modeling periodic systems, the simulation cell needs to be charge neutral to avoid the divergence of electrostatic contributions. In partially periodic systems, it is also possible to mimic image charges by changing the boundary conditions of the Poisson equation. The ionic distribution obtained by solving the mPB equation provides a physically and chemically sound method to neutralize the cell, making mPB models highly attractive. However, in practice, the neutralization from mPBs is incomplete and significant charges can remain in the simulation cell even after the mPB distributed ions are added.[32] The charge neutrality constraints are not built in the mPB models and their simple form does not guarantee charge neutrality even if large simulation cells are used in typical mPB simulations.[71] While a physically correct model should yield charge neutrality automatically, the restricted form of the mPB necessitates the use of additional constraints. The traditional way of neutralizing the cell is to add a homogeneous background charge, which will create spurious interactions and incorrect energetics unless corrections are applied.[21] To avoid the use of homogeneous background charges, two alternatives are presented.

1. The Lagrange multiplier approach

Modifying the ion distribution provides a chemically justified approach to the overall charge neutrality. The overall neutrality condition is $\int d\mathbf{r} \rho(\mathbf{r}) = \int n(\mathbf{r}) + \rho_\pm - N(\mathbf{r}) d\mathbf{r} = \int n_{dft}(\mathbf{r}) + \rho_\pm d\mathbf{r} = 0$. For the models considered in this work, the charge neutrality condition has the form

$$Q_{dft} + \int g(\mathbf{r}) \sum_i z_i c_i(\mathbf{r}) d\mathbf{r} = 0, \tag{33}$$

where $g(\mathbf{r})$ is an exclusion (cavity) function determined in Sec. III. An additional Stern exclusion layer within Simple Continuum Model based on Volumetric Data (SCMVD) is simply $c_i^{ex} = (g(\mathbf{r}) + f(a))c_i$ using experimentally defined ion radii a.

In general, the ion concentration can also be written in terms of the ion chemical potential which is obtained by minimizing the grand potential with respect to the ion density resulting Eqs. 10(a)–10(c) of the supplementary material. For example, in the Gouy-Chapman model, $\mu_i(\mathbf{r}) = \beta^{-1} \ln[\lambda^3 c_i(\mathbf{r})] \exp[-z_i \beta \phi(\mathbf{r})]$. The cavity factor $g(\mathbf{r})$ can be interpreted as the effective pair-density functional which depends on the total interactions between the DFT subsystem and the liquid (see Sec. III). Keeping this analogy, we can write the total number of ions to fulfill the neutrality constraint as

$$
\begin{aligned}
-Q_{dft} &= \int g(\mathbf{r}) \sum_\pm z \exp[\mu_\pm \beta] \exp[\mp \beta |z| q \phi(\mathbf{r})] d\mathbf{r} \\
&= \int \exp[u_{eff}(\mathbf{r})\beta)] \sum_\pm z \exp[\mu_\pm \beta] \exp[\mp \beta |z| q \phi(\mathbf{r})] d\mathbf{r} \\
&= \int \exp[u_{eff}(\mathbf{r})\beta)] \sum_\pm z \exp[\beta(\mu_\pm^{PB} + \mu_\pm^0(\mathbf{r}))] \\
&\quad \times \exp[\mp \beta |z| q \phi(\mathbf{r})] d\mathbf{r}.
\end{aligned} \tag{34}
$$

The $\mu_\pm^{PB}$ term accounts for assumptions of the interactions used for deriving the ion distributions in the (modified) PB models. It can also be seen as a Lagrange multiplier to enforce the bulk concentrations as $\phi \to 0$. The additional term $\mu_\pm^0(\mathbf{r})$ can be considered as a Lagrange multiplier to enforce charge neutrality[32] or interpreted as an excess chemical potential corresponding to the interaction between the ions and the DFT subsystem. It is stressed that this additional chemical potential can be an ion-dependent local function affecting either the effective potential, cavity function, or the chemical potential of the PB ions.

The simplest choice for the neutralizing Lagrange multiplier would be $\mu_\pm^0(\mathbf{r}) \approx \mu^0$, and the multiplier would be the scaling factor $\mu^0 = \ln[-Q_{dft}/Q_\pm]$. A second option is $\mu_\pm^0(\mathbf{r}) \approx \mu_\pm^0 = \mu_\pm^0$, the simplest choice being $\mu_+^0 = -\mu_-^0$. Then, the neutrality constraint results in

$$Q_{dft} + Q_+ \exp[\mu^0\beta] + Q_- \exp[-\mu^0\beta] = 0, \qquad (35a)$$

$$\mu^0 = \beta^{-1} \ln\left[\frac{\sqrt{Q_{dft}^2 - 4Q_+Q_-} - Q_{dft}}{2Q_+} \right], \qquad (35b)$$

which was also derived and applied in Ref. 32 and subsequent work.

The physicochemical implications of the neutralization conditions above can be understood by studying the behavior of charge neutralized PB-equation deep in the liquid and to meet the conditions set by $\mu_\pm^{PB}$. The ionic charge density should be zero in order to respect charge neutrality in bulk electrolytes. The choice of boundary conditions for the PB equation guarantees that electrostatic potential approaches zero. Also, g approaches unity by construction of the cavity function. Then ion concentrations for position independent excess chemical potential follow

$$\rho_\pm^\infty = \sum_i c_b z_i \exp[\beta(\mu_\pm^0 \mp \phi)] \approx \sum_i c_b z_i \exp[\beta\mu_\pm^0] = 0. \qquad (36)$$

If $\mu_\pm^0 = \mu^0$, the ion density from above approaches zero correctly. However, the ion concentrations do not yield the correct bulk values and instead $c_i = \exp\mu^0 c_b$ is obtained. For the asymmetric constraint $\mu_+^0 = -\mu_-^0$, the above results in equation will give $\rho_\pm = -2\sinh[\mu^0]$ and $c_\pm = \exp|\mu_\mp^0|$. Thus the bulk electrolyte is not reached even far away from the electrode, and situations are not ideal for the electrochemical setup.

Instead, such a situation is encountered when the electrode and nearby electrolyte solution would be isolated from the bulk liquid by a semi-permeable membrane which allows exchange of ions but not the electrode or reactant nuclei.[71,72] This corresponds to an electrochemical equilibrium of ions across the membrane such that the ion and potential gradient is formed; this is the Donnan equilibrium where a potential difference $\phi_{Donnan} = (RT/zF)\ln[c_{in}/c_{out}]$ builds over the membrane.[73] In Donnan equilibrium, the ion concentrations have the form

of Eq. (36) which are determined by the *difference* $\varphi(x) = \mu_\pm^0 \mp \phi(x)$ (called gauge-invariance in Ref. 71). In the electrochemical setup, this is problematic as $\varphi(\infty) = 0$ is guaranteed, but *the choice of absolute values of $\mu_\pm^0$ and $\phi(x)$ is arbitrary*. As an example, if one chooses $\mu^0 = 0$ and imposes the charge neutrality condition, $\phi^S = \phi_{Donnan}$, and the reference electrode discussed in Sec. II E should be $\phi^S + \phi_{Donnan} = \phi(\infty) = 0$ and ϕ_{Donnan} would be the boundary condition for the PB equation. If $\phi^S = 0$ is taken as the reference, the bulk ion densities are not obtained and the free energies would be affected. Thus, enforcing the position independent Lagrange multiplier for the neutrality condition destroys either the reference electrode in the liquid, the ion density constraint of bulk charge neutrality, or both.

In Ref. 74, it was concluded that the charge-neutrality condition leads to breaking the spatial independence charge distribution. In other words, only a position-dependent multiplier can satisfy the correct ion density and concentration as well as electrostatic potential limits far from the DFT region. Choosing a local ion independent constraint, $\mu_\pm^0(\mathbf{r}) \approx \mu^0(\mathbf{r})$, will effectively result in an ionic cavity function which depends on the charge state of the DFT subsystem. This would likely allow the ions to penetrate deeper in the DFT region. Thus, ions would reside within the solvent cavity resembling specific adsorption which is outside the applicability of PB-like approaches as highlighted while deriving the continuum GC-DFT approach. Also large ion concentrations would be observed close to the nuclei. These considerations apply also to ionic exclusion models presented in Refs. 37 and 29.

Still, such ion-independent spatial correction approaches were suggested in Ref. 75 to account for specific adsorption and in Ref. 74 to derive a charge-conserving Poisson-Boltzmann equation by including a "charge-trap region" near the electrode surface. Bound ions can also be considered as an effective way to renormalize the surface charge by ion adsorption to enforce global charge neutrality.[76]

Phenomenologically, the above methods where the neutralizing charge is confined near the electrode can be seen as a Stern layer-type correction with tightly bound ions. However, the underlying mPB models are derived for classical nuclei, as discussed in Sec. II C, and no real bonds can form between classical and quantum parts of the system. Thus, the strong chemisorption is not within the assumptions included in mPB models and the applicability of this neutralization approach is questionable. Also for a heterogeneous system, the neutralizing charge should not be homogeneous or lie in the low dielectric region but rather reside in the regions of high dielectric to correctly describe the gradient of the electrostatic potential correctly.[77] In the above methods, the ion density mimicking strongly bound ions in the Stern layer would result in ions inside the cavity ($g(r) < 1$, $\epsilon(\mathbf{r}) < \epsilon(bulk)$) where dielectric constant is low. Thus, the artificial Stern layer might have an adverse effect on the description of the interfacial potential distribution.

Capturing the interfacial potential drop is important for an electrochemical experiment, and therefore ion distribution close the interface should remain unaffected by enforcing the neutrality. Far away from the electrode, the ion concentration is small and the potential profile is rather flat, making it safer to place the neutralizing ions in the high dielectric region. A simple form for an augmenting potential fulfilling these properties is

$$\mu\beta = \ln(\gamma_\pm c_\pm(\mathbf{r})) = \ln(\gamma_\pm \lambda^3(c_b + c_\pm^0(\mathbf{r})))$$
$$= \ln \gamma_\pm \lambda^3(c_b + c_\pm^0 \theta(\mathbf{r})), \qquad (37)$$

where γ is the activity coefficients accounting for finite-size effects, interactions beyond electrostatics, etc., which can be used to arrive at different modified PB models. Setting $\gamma = 1$ corresponds to an ideal ionic liquid which can be treated with the Gouy-Chapmann model. Using these definitions, we obtain

$$\Delta Q = \int \sum_\pm z_\pm \gamma_\pm c_\pm^0 g(\mathbf{r})\theta(\mathbf{r}) \exp[\mp\beta|z_\pm|q\phi(\mathbf{r})]d\mathbf{r}$$
$$\rightarrow c_\pm^0 = \frac{\Delta Q}{V_\pm}. \qquad (38)$$

To arrive at the final expression, we write ion distribution as

$$\rho_\pm(\mathbf{r}) = g(\mathbf{r}) \sum_\pm \frac{z\left(\exp[\mu_\pm^{PB}\beta] + \dfrac{\Delta Q}{V_\pm}\right)}{\lambda^3} \exp[\mp\beta|z|q\phi(\mathbf{r})]$$
$$= g(\mathbf{r}) \sum_\pm (c_b + c_{cor}(\mathbf{r})) \exp[\mp\beta|z|q\phi(\mathbf{r})]. \qquad (39)$$

When the volume of the ion density is large, the correction term becomes small. The function can be interpreted as either locally increasing the concentration or charge of the ions. Also, the function defining the excess chemical potential leading to neutralizing ion density $\theta(\mathbf{r})$ needs to approach zero far away from the DFT subsystem in order to yield bulk ion density and concentrations. Probably, the simplest choice is to make $\theta(\mathbf{r})$ a smooth step function to equal zero at the boundaries, but this choice is rather arbitrary.

The neutralization condition can also be extended to the solvent mimicking solvated ions, leading to a uniform neutralizing charge outside the solute cavity residing only in the high dielectric region.[77] Such an assumption seems nonphysical as the neutralizing "ions" would not feel the electrostatic potential of the solute. Surprisingly, such an approach has been successfully applied to the computation of potential of mean force profiles which are directly linked to the interaction of the solvent and ions with the surface. A comparison of classical molecular dynamics with homogeneously distributed charge in the high dielectric regions mimicking charging of water molecules has shown to yield potential of mean force profiles comparable to explicit ion simulations.[77]

Given that such a simple homogeneous neutralization successfully mimics explicit ions, a simple way of simulating

charged cell is obtained by homogeneous neutralization of the solvent region. Indeed, in very recent independent work by Pettersson,[33] such an approach, called the solvated-jellium model (SJM), was developed, utilized, and implemented in the GPAW code used also in this work. SJM provides neutralization and also establishes a convenient reference electrode as detailed in the present work, but the *ad hoc* nature of the jellium counter charge requires testing and comparison to other methods.

2. Modified boundary condition approach

An alternative way to study charged partially periodic cells is to modify the underlying electrostatic problem by selecting convenient boundary conditions for the PB equation. A common computational setup in model systems used for studying the double-layer behavior is a parallel-plate capacitor where both plates are placed at $z = \pm L$ carrying opposite but otherwise equal charge densities. Also, in the absence of ion-specific effects, the double-layer densities are identical but carry opposite charges. Thus, the overall system is naturally charge neutral.

In a practical DFT calculation, the presence of two electrodes is not feasible due to the increased computational cost nor desirable as one is usually only interested in half-cell reactions. A convenient work-around is to treat the total system using the method of images and to use the image as a neutralizing charge. By imposing a condition that $\phi^S(z = 0) = 0$ between the plates, a reference electrode can be restored. For simple model systems where analytic solutions are available, the electrostatic potential from the image charge method (in the relevant regions) is equal to placing a perfect conductor at $z = 0$ as an imaginary electrode.[57] The system polarizes the imaginary electrode, and the charge polarization restores charge neutrality of the simulation cell. Also the electrostatic potential at the imaginary electrode is $\phi^S = 0$.

The imaginary electrode method is equal to the effective screening method (ESM) pioneered by Otani and Sugino[16] to remove periodic boundary conditions in one direction in otherwise periodic plane-wave calculations. The essential outcome from the ESM is a derivation of analytic boundary conditions for the Poisson equation in charged systems. If an asymmetric simulation cell is used, as usually performed in the presence of adsorbates or reactants, the imaginary electrode needs to be placed on the "active side" of the real electrode to obtain the correct zero electrostatic potential reference on the correct side. To internally reference against the vacuum potential, the gradient of the electrostatic potential is taken to approach zero on the inactive side (see discussion at the end of Sec. II E). Also care needs to be taken that the electron/ion density is vanishingly small at the ESM boundary and that enough vacuum is inserted at the cell boundary.

In real-space approaches, such as the grid-base in GPAW[78,79] utilized in this work, the unit cell can be truly non-periodic and zero electrostatic boundary conditions in

non-periodic directions are commonly employed when solving the Poisson equation. In the supplementary material, we detail how ESM-like schemes can be implemented in real-space codes by numerically approximating the ESM Green functions to enable calculations of charged unit cells. In asymmetric systems, the dipole correction[80] is applied to give asymmetric electrostatic potentials, leading to the different work functions on different sides of the slab. In the original dipole correction scheme, a correcting potential is introduced,

$$V_{dip}(z) = 4\pi m \left(\frac{z - z^0}{z_m} \right), \tag{40}$$

where $m = \int_{-\infty}^{\infty} dz' \rho_{av}(z')(z' - z^0)$ is the surface dipole density referenced to z^0 which in the present case is chosen to be on the active side of the system to satisfy either $\phi(z^0 = 0) = 0$ or $\phi(z^0 = z_m) = 0$. Although undocumented, GPAW uses a modification of the original dipole method and a potential $V_{dip}(\mathbf{r}) \sim m \, \mathrm{erf}(\mathbf{r})$ is used instead of a saw-tooth potential of the original dipole correction. As shown in the supplementary material, the dipole correction combined with the standard multi-grid Poisson solver can be used to numerically (and accurately) approximate the ESM Green functions. In the presence of mPB ions, the only modification needed is the inclusion of ion densities in the total charge density with ion density restricted to exist only on the active side.

Ideally both the electrostatic potential and its gradient should be zero on the *active* side of the electrode to obtain the correct behavior of the ionic distribution, but such Cauchy boundary conditions do not give a unique solution of the PB equation,[57] and thus the correct gradient is sacrificed in the boundary condition approach. Note that true non-periodicity is exclusive to real-space methods because the potential does not have to be periodic in the desired direction. In plane-wave calculations, $z^0 = z_m/2$ needs to be chosen to make the potential periodic in all directions and extrapolation of the potential is needed as discussed in Ref. 16.

III. IMPLEMENTATION

The theoretical concepts derived above for the classical continuum electrolyte are implemented as part of the GPAW code[78,79] which uses the projector augmented wave (PAW) method[81] for replacing the rapidly oscillating KS wave functions by smooth pseudo-wave functions near the nuclear regions. More specifically, the Simple Continuum Model based on Volumetric Data (SCMVD)[59] already implemented in GPAW is augmented with new features for treating charged periodic systems using modified Poisson-Boltzmann models and the boundary condition method closely related to the ESM.[16]

A. Poisson-Boltzmann model with SCMVD

SCMVD belongs to a class of implicit solvation models where a quantum subsystem (often called the solute) is immersed in a dielectric continuum. For completeness, the original SCMVD method is detailed in the supplementary material, while here only the modifications needed for mPB simulations are needed. SCMVD utilizes a linear dielectric

function of the form

$$\epsilon[g(\mathbf{r})] = 1 + (\epsilon_\infty - 1)g(\mathbf{r}), \tag{41}$$

where $g(\mathbf{r})$ is the effective pair distribution function of the solvent in the presence of the solute. $g(\mathbf{r})$ is zero close to the solute and increases smoothly to unity. Since our focus is to combine classical continuum and electronic GC-DFT for describing electrochemical interfaces, it is appealing that the dielectric is a functional of the cavity function which can be interpreted as pair-density function used widely in the DFT of classical fluids.[7]

We modify the original SCMVD dielectric to account for local screening by the ions in solution and to include changes in the water dipole orientation due to the external potential created DFT region. Together these terms can be accounted by the ionic decrement,[60,61,65]

$$\epsilon[\rho_\pm(\mathbf{r})g(\mathbf{r})] = 1 + (\epsilon[\rho_\pm(\mathbf{r})] - 1)g(\mathbf{r}), \tag{42}$$

where $\epsilon[\rho_\pm]$ replaces ϵ_∞ to account for the dielectric treatment due to ion accumulation,

$$\int d\mathbf{r}(1 - g(\mathbf{r})) = v_M^\infty - \kappa\beta. \tag{43}$$

The effective potential in the original SCMVD implementation was chosen to have the form

$$g(\mathbf{r}) = \exp[-\beta u(\mathbf{r})], \tag{44a}$$

$$u(\mathbf{r}) = u_0 \sum_a \left[\frac{R_a^{vdW}}{|\mathbf{r} - \mathbf{R}_a|} \right]^{12}, \tag{44b}$$

where $u(\mathbf{r})$ is the effective pair-potential. We stress that $\epsilon[g(\mathbf{r})]$ does not depend on the electron density which circumvents numerical instabilities and makes electrostatic potential particularly simple. This point was also stressed in the recently developed soft-sphere continuum method[34] and its adaptation.[37] SCMVD and the soft-sphere cavities are very similar.[34] The form of the cavity guarantees that the computation of non-electrostatic terms consisting of cavitation, repulsion, dispersion, and changes in rotational/translation free energies of, i.e., the chemical interactions presented in Eq. (23) is straightforward, as shown in the supplementary material.

The next step toward treating an electrolyte in contact with a surface is to add the ions to the solution. We note that the implicit solvation model of an electrolyte is best suited for situations where specific adsorption of the ions does not occur as has been discussed in Sec. II. In this case, the electrolyte forms a diffuse double layer, also called the Gouy-Chapman layer. In Sec. III, we showed how the Gouy-Chapman model can be made more general by including the finite size effects, the Stern layer, and ion solvation terms. The effect of both terms is to prevent unphysical charge build-up near the surface and also account for ion specific interactions. Still they are not capable of treating specific adsorption of ions, and to account for this, the ionic density of the electrolyte is excluded from the cavity. Ion exclusion is efficiently achieved by multiplying the ion distribution with a function that goes to zero

within the cavity.[35,37,59] In the absence of a separate Stern exclusion layer, natural choice is the effective potential $g(\mathbf{r})$. If a Stern layer is present, it is simple to make the replacement $g(\mathbf{r}) \rightarrow (g(\mathbf{r}) + f(a))$. Without further specifying whether or not the Stern layer is accounted for, the ion concentration including the exclusion is

$$c_i^{ex}(\mathbf{r}) = g(\mathbf{r})c_i(\mathbf{r}). \qquad (45)$$

If ion solvation effects are neglected, ion distributions have the form of the Gouy-Chapman,

$$c_i(\mathbf{r}) = c_b \exp(-\beta z_i q \phi(\mathbf{r})). \qquad (46)$$

For small potentials, the GC model can be linearized to yield

$$c_i^{lin}(\mathbf{r}) = \beta c_b q z_i \phi(\mathbf{r}). \qquad (47)$$

Gouy-Chapman and its linearized form are the most widely used and simplest approaches for including the electrolyte in implicit solvation models.[25,31] Both are based on the assumption that the ions are point-like, which can lead to overestimation of ionic concentration close to the charged surface at high potentials and/or high (>1M) concentrations. The simplest way to account for the finite-size effects is the Bikerman-Freise equation[63] for a symmetric binary salt,

$$c_{\pm}^{BF}(\mathbf{r}) = \frac{c_b \exp[\mp\beta|z|q\phi(\mathbf{r})]}{1 + 4a^3 c_b \sinh^2(\beta z_i q \phi(\mathbf{r})/2)}. \qquad (48)$$

Ion specific effects can also be incorporated using the ion decrement model of Eqs. (25). Inserting the decrement term from Eq. (21) and utilizing Eq. (42) lead to a mPB equation with both ion decrement and finite size effects,

$$\mathcal{C}_{\pm}(r) = c_b \exp\left[\mp\beta z e \phi - \frac{\beta g(\mathbf{r})\alpha_{\pm}}{8\pi}|\nabla\phi|^2\right], \qquad (49)$$

which is inserted in (25).

B. Solving the generalized Poisson-Boltzmann equation

The non-linear character of the mPB equation places pressure on the Poisson solver. In GPAW, all potentials and wave functions are presented on a real-space grid and the Poisson equation is solved using multigrid techniques.[78,79] As GPAW works in real-space, the simulation cell can be chosen to be either truly periodic or non-periodic. All calculations where the mPB models are applied are at least partially non-periodic; slab, wire, and molecule calculations are 2D, 1D, and 0D periodic, respectively.

To meet the increased complexity arising from the non-linearity of the PB differential equation, the standard Poisson solver in GPAW was augmented with the recently developed algorithms of Ref. 30. Specifically, we have implemented the

self-consistent PB algorithms with self-consistent (SC) iterative procedure (algorithms 1 and 3 of Ref. 30). We used a mixing parameter of 0.6. To connect with the boundary condition method for solving the Poisson equation, we note that all the mPB calculations use method (i) of the supplementary material. In these mPB calculations, a symmetric unit cell and the dipole are zero.

Following the discussion in Sec. II F, a charged system can be modeled either by enforcing charge neutrality using a (chemically motivated) Lagrange multiplier or by modifying the boundary conditions of the underlying Poisson solver. When using the Lagrange method, Dirichlet boundary conditions with $\phi(boundary) = 0$ are chosen in the non-periodic directions. In the modified boundary condition method, Dirichlet boundary conditions with $\phi(boundary) = 0$ are chosen for the active side and the other boundary is determined from the dipole correction.[80]

We use the modified boundary condition method for simulating a charged unit cell in the presence of a dielectric liquid but without the presence of mPB ions. The purpose is to compare mPB models with a model where the charge neutrality is obtained by image charges obtained from the modified boundary conditions of the Poisson equation. In the calculations, we utilized the boundary condition iii of the ESM[16] in the presence of a dielectric. The practical implementation of the boundary condition method is detailed in the supplementary material.

IV. COMPUTATIONAL DETAILS

All calculations are carried out using the GPAW code[78,79,82] and the PBE[83] functional. The grid-spacing is set to 0.18 Å, and the geometry of all systems is fully optimized until the force is <0.05 eV/Å. The convergence criterion for the electronic SCF is 10^{-5} eV/atom. An mPB model is considered converged when the maximum difference between ionic density and successive iterations is below 10^{-12} Å^{-3}. $4 \times 4 \times 1$ k-point sampling was used in all calculations. The z-direction of the simulation cell is $3\kappa_D^{-1}$, where κ_D^{-1} is the Debye screening length. Parameters for the ion decrement and finite ion size mPB models were taken from Ref. 60: the ion diameter for Na (F) is 7.16 (7.04) Å, while the linear decrement coefficient is 8. (5.) dm^3/mol. When including the Stern layer, the reported values used an ionic exclusion radius smaller than the ion diameter: 3.5 Å. Smaller and larger exclusion radii were also tested, but the results were similar and therefore not shown. The chosen Stern radius used for NaF is close to that of NaCl, as determined from *ab initio* molecular dynamics (AIMD) in Ref. 29. For all but the modified boundary condition method, a symmetric simulation cell with dielectric/electrolyte on both sides was used. This is accounted for in the calculation of the capacitance.

The cavity shape parameters to form $g(\mathbf{r})$ and the effective surface tension are taken from Ref. 59. The parameters are fitted for main group elements and might not be suitable for the metallic surfaces considered in this work. The

computational focus of this work is not on the quantitative description of energetics but on the qualitative performance of the mPB models. The main parameter affecting the electrostatic potential and double layer capacitance considered in this work is the van der Waals (vdW) radius used for defining the cavity. In the original SCMVD implementation and the recent SJM model, the vdW radii by Bondi[84] were used, and the Au radius is 1.66 Å. However, the Bondi vdW radii are determined for non-metallic compounds or metal-organic molecules and might therefore be unsuitable for the treatment of the metal-water interface. Indeed, crystallographic data on metallic Au systems indicate that the vdW radius is larger and around 1.9 Å.[85] During this study, we found that the double-layer capacitance sensitively depends on the used vdW radius. We therefore determined the distance between the metal and water from a planar distribution function (PDF) obtained from an *ab initio* molecular dynamics simulation, as detailed in the supplementary material. From the PDF, we can conclude that the Au–H half-peak is found at distance of 2 Å. For comparison, all data were computed using vdW radii of 1.66 and 2.00 Å. A more complete parameterization for metallic surfaces is currently in process.

Two different cavity radii were tested: (i) 1.66 Å Bondi vdW radius as performed in the original SCMVD article[59] and in the recent SJM model[33] and (ii) 2.00 Å obtained in this work from AIMD simulations. Several different methods for treating the continuum ion distribution models, namely, linearized, Gouy-Chapmann, Bikerman-Fraise, and ion-decrement mPB were utilized. For all the models, different neutralization schemes were also studied and we used the Donnan Lagrangian method of Eq. (35a), uniform neutralization in the dielectric, and modified double layer scheme of Eq. (39) with a smooth step function in order to reach the bulk ion concentration at the cell boundary. Also simplified ion distributions, namely, the uniform jellium in the dielectric in the spirit of SJM[33] and Gaussian charge sheets as performed in Ref. 86, were tested. The modified boundary condition method without neutralizing ions in the spirit of ESM[16] was studied for comparison.

All calculations are naturally grand canonical for the ions while the electronic degrees of freedom have been treated within the canonical ensemble. A simple grand canonical calculator for the electronic system in the spirit of SJM[33] was also implemented. Also, a constant-μ method by Otani[17] was implemented in the ASE code.[82] Testing efficiency and performance of different constant electrode potential methods is the subject of ongoing work, but here we focus on the description of the electrode-electrolyte interface under various computational schemes in the electronic canonical ensemble.

V. STUDIED SYSTEMS

Using the outlined classical continuum grand canonical scheme for electrons and the electrolyte, we study the differential capacitance (C_d) of well-defined single crystal metal electrodes in aqueous solutions. Specifically, we study the surface capacitances and interfacial potentials of the Au(210) surface in a 0.5M NaF solution.

The differential capacitance is a sensitive but indirect measure of the electrode-electrolyte interaction. As shown in Fig. 1 of the supplementary material, both the magnitude and shape of the experimentally measured differential capacitance curves of Au(210) in NaF electrolyte solutions depend sensitively on the surface charge and electrolyte concentration. The differential capacitance is defined as

$$C_d = \left(\frac{\partial \sigma_m}{\partial E} \right)_{\mu_i^S, T, V}, \tag{50}$$

where σ_m is the surface charge density of the metal. A particular point where $\sigma_m = 0$ is the PZC. Now it must be noted that the capacitance is specific to a given electrolyte and as such also PZC depends on the electrolyte and its concentration. Since the mPB model is suitable for treating the diffuse electrical double layer, an electrolyte without specific adsorption should be chosen to avoid issues related to partial charge transfer (see Sec. II B for related discussion. Using experimental values for PZC in different solvents and electrolytes allows one to connect the PB solvent with a real electrolyte by finding $\Delta \chi_S$ of the electrolyte.

It is important to bear in mind that in linear and Gouy-Chapman mPB models, all ions are point-like, while in the BF-model, the ions have a finite size but neither model affects the dielectric and only the pure solvent dielectric constant is utilized. Therefore it is expected that $\Delta \chi_S$ is equal for all ions in the Gouy-Chapman and BF models. On the other hand, in the dielectric decrement mPB, the dielectric constant does not equal that of the pure solvent but depends linearly on the ion concentration. Thus, $\Delta \chi_S$ in the dielectric decrement model is, in principle, ion and concentration dependent. The effect of ion density and dielectric decrement on surface potentials is of the order ~±10 mV for 1:1 electrolytes when the concentration is under 6 mol/dm³.[87] Therefore, $\Delta \chi$ and the reference electrode are equal for all solvent models considered in this work (however, the value may depend on the used vdW radii defining the cavity).

In addition to capacitances, we also study the interfacial electrostatic potentials obtained from different schemes. Correct behavior of the electrostatic potentials at different electrode charges and potentials is paramount for describing the electrochemical cell.

VI. RESULTS AND DISCUSSION

A. Differential capacitance of Au(210) in 0.5M NaF

Here we focus on the most important features of the computed surface capacitance profiles from different methods. The detailed surface-charge–electrode potential plots for several tested combinations are presented in the supplementary material. A representative example is presented in Fig. 3.
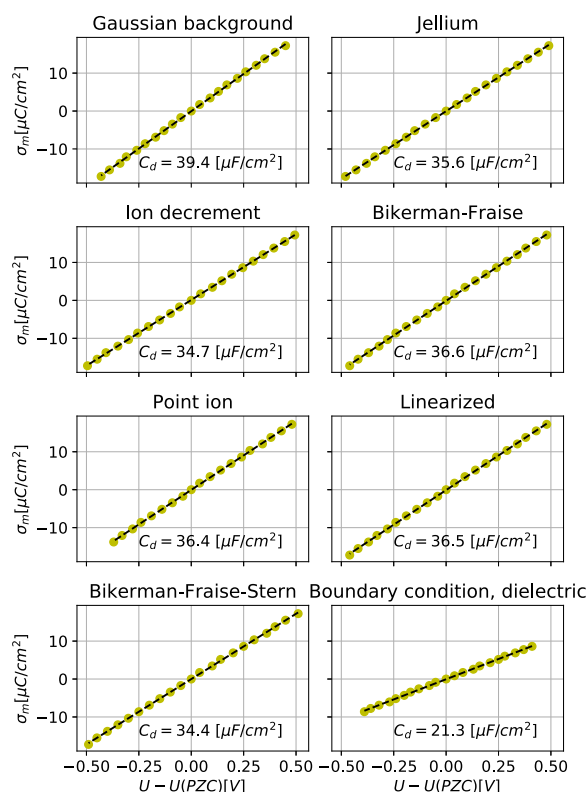
FIG. 3. The Fermi-level plotted at different surface charges σ_m using different mPB models. The dots present the computed data points, and the black line is a linear fit. The differential capacitance C_d is obtained from the slope of the linear fit. The Donnan neutralization method is used, and the Au vdW radius is set 2.00 Å.

The main finding is that, regardless of the mPB model, only constant capacitances are obtained from the calculations. This is in contrast to the experimentally obtained curve which has a distinct bell-like shape peaking at the PZC around 65 μF/cm^2 and declining to 25 μF/cm^2 at around ±0.5 V from PZC, as shown in Fig. 1 of the supplementary material. It is unlikely that the differences are caused by the choice of the F-anion as almost identical differential capacitances are obtained for Au(210) in NaBF$_4$ solutions.[88] The constant value for the simple models such as the Gaussian and jellium[33] as well as linearized,[31,37] point-like Gouy-Chapman is expected in a linear dielectric model. However, the quantitatively similar linear behavior for the finite-size Bikerman-Freise model has not been shown before. Also the inclusion of the Stern layer does remedy the linear behavior in the linear dielectric model used. It is surprising that the ion-decrement model also predicts constant differential capacitance when coupled with SCMVD and DFT as this model can produce both maxima and minima of the capacitance in simple classical models.[60,61] A plausible reason for poor performance of the dielectric decrement model is the need to enforce charge neutrality as discussed below and the use of a cavity function. Even if the capacitance is not improved by increasing the complexity and

including more ion-specificity, the energetics are expected to be improved in the more complicated mPB models.[29]

While the shape of the differential capacitance does not depend on the chosen method, the absolute values of the capacitance are more sensitive. When using the Bondi ion radius of 1.66 Å, the capacitance is ~65 μF/cm^2 for the Gaussian sheet and linearized, Gouy-Chapman, and Bikerman-Fraise PB models. In the jellium and ion decrement models, the ion distribution is more diffuse and the differential capacitance is ~55 μF/cm^2. Capacitance from the modified boundary condition is much lower: 30 μF/cm^2. When using a larger Au radius (2.00 Å) determined from AIMD simulations, smaller capacitances are observed. As before, smaller capacitances are obtained from jellium and ion decrement models, but the spread is smaller, and the capacitance is within 34–40 μF/cm^2. The boundary condition method is still an outlier giving the capacitance of 22 μF/cm^2. Finally, we note that capacitances as obtained using the larger vdW radius are within 20–30 μF/cm^2 in agreement with other mPB models[25,31,37] and explicit ice-like–water structures.[24,89]

From the study of different neutralization schemes, one can conclude that the obtained capacitances depend mildly on how the system is neutralized. The modified double-layer and Donnan Lagrange neutralization methods give nearly identical results, while the uniform dielectric neutralization produces slightly smaller capacitances. There is an important exception, though: in the ion decrement model, the neutralization method changes the overall ion distribution and therefore affects the dielectric in an unexpected way: even for the modified double-layer and Donnan method, the neutralization introduces a smooth ion density in the simulation cell. Also changes in the dielectric due to decrement exhibits an almost constant decrease instead of pronounced spatial dependence. An example is shown in Fig. 4.

B. Electrostatic potentials from different schemes for Au(210) in 0.5M NaF

The interfacial potential is an important factor in electrochemical systems affecting both reaction thermodynamics and kinetics. To relate the electrostatic potential and
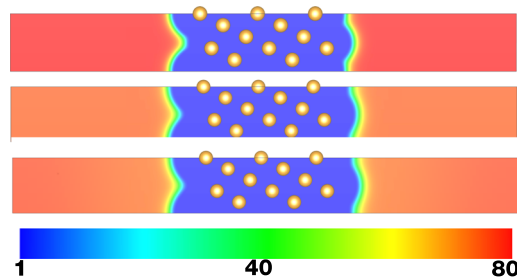
FIG. 4. From top-to-bottom: (1) Dielectric profile without decrement, (2) dielectric profile with dielectric decrement in 0.5M NaF using the uniform neutralization, and (3) dielectric profile with dielectric decrement in 0.5M NaF using the scheme. The color scale at the bottom varies from ϵ = 1 (blue) to ϵ = 78.36 (dark red) of normal bulk water.
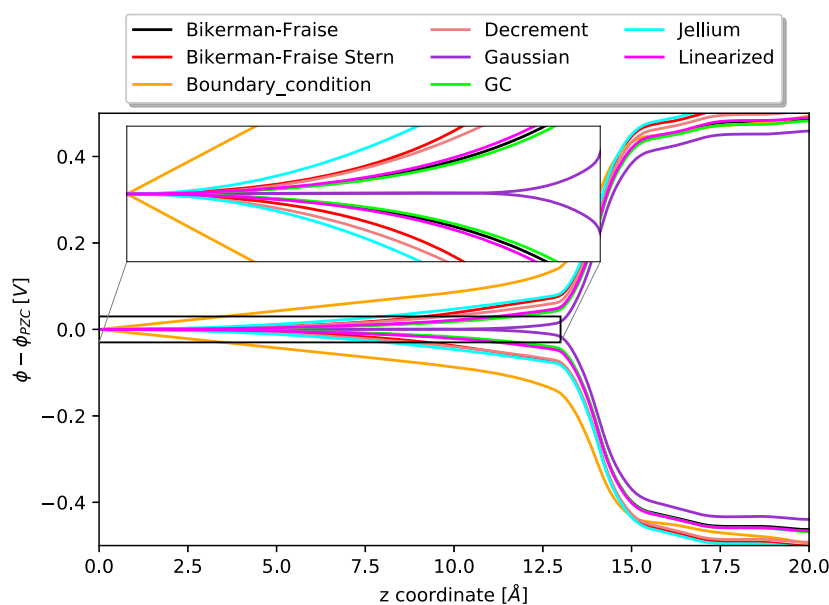
FIG. 5. The interfacial electrostatic potentials from different schemes. Above the PZC, the potential is set to 0.5 V and below to −0.5 V vs. PZC. The inset highlights the long-range behavior. The top most atom is located at 16.5 Å. The Donnan charge neutralization was used, and the vdW radius is 2.00 Å. The bulk electrolyte is reached at z = 0.

electrochemical potential of electrons from the computational models to experimentally utilized reference electrodes, schemes from Sec. II E need to be used. Instead of referencing the potential against reference electrodes, computational studies[36,37] of electrochemical systems have used PZC as an internal reference which is afterwards[25,31–33] calibrated to the SHE reference via the experimental PZC on the SHE scale. The calibration value depends on the used solvent model: for models where the dielectric cavity depends on the electron density as $\sim$erfc[log($n(\mathbf{r})/n_c$)] such as CANDLE,[32] VaspSOL,[31] and linear PCM,[25] absolute SHE is calibrated to be between −4.4 and −4.7 V, but for the soft-sphere or SCMVD type of models, such a calibration is not available.

The experimental value[90] for PZC of Au(210) in a 0.5M NaF is 0.144 V vs. SHE. In our modified SCMVD model, the absolute potential is simply $-E_F$, as discussed in Sec. II E. By studying the two different radii for the dielectric/cavity (at which the dielectric and ionic density difference also start differing from zero), we notice that the Fermi-level of the neutral Au(210) depends sensitively on the used radius. For R = 1.66 Å, $E_F(\sigma_m = 0) = -4.27$ V, and for R = 2.00 Å, $E_F(\sigma_m = 0) = -4.71$ V. Thus, calibration for R = 1.66 Å is −4.41 V and for R = 2.00 Å is −4.84 V. Both are close to the values obtained from electron density dependent cavities and the experimentally determined absolute SHE value which varies from −4.4 to −4.85 V.[91] As discussed, the calibration is closely linked to the used cavity radius which in turn determines the computed differential double layer capacitance. Therefore a judicious choice would to choose the vdW radius for the dielectric/cavity which reproduces the experimentally obtained capacitance and afterwards fix the calibration between the Fermi-level and PZC from comparison experiment and computations.

Given the dependence of the absolute potential on the used vdW radius, we report on the electrostatic potential profiles in Fig. 5 with respect to the PZC of a given model. First, the electrostatic potential obtained from the boundary condition method decreases to zero slower than all other methods and the gradient is nonzero, as expected. Similar behavior was observed also with the similar ESM.[16] Of the used mPB models, linearized PB, Gouy-Chapman, and Bikerman-Fraise produce almost identical and overlapping potential curves. When the Stern layer is added (shown for Bikerman-Fraise), screening is delayed but is otherwise similar to the underlying mPB. The electrostatic potential from Gaussian charge sheet depends sensitively on the position and width of the sheet. Here, it is seen to screen the charge faster than the mPB methods, whereas the uniform jellium screens the charge slower.

As discussed above, the charge distribution from the ion decrement is rather homogeneous and also the resulting potential is rather similar to the one obtained from the jellium models or when the Stern layer is included. However, the ion decrement approach is the only model for which the interfacial electrostatic potentials are not symmetric for positive and negative potentials vs PZC. At positive potentials, the ion decrement model predicts slightly stronger screening which reflects the higher dielectric, i.e., smaller dielectric decrement, of the fluoride anions building at the surface at positive potentials.

VII. CONCLUSIONS

We have presented a general density functional theory framework for modeling electrochemical interfaces at fixed electrode and ion potentials. Our approach provides a rigorous ion/electron grand canonical ensemble DFT relevant to electrochemical systems. This allows one to perform

atomistic simulations of electrochemical interfaces using experimentally meaningful control variables, namely, the electrode and ion chemical potentials, solvent, and temperature. Such simulations will advance the understanding and optimization of electrochemical interfaces.

Besides the general framework, a systematic coarse-graining from a fully quantum mechanical nuclei and electrons to classical nuclei of the electrode, ionic and solvent nuclei interacting with electrons, and continuum electrolyte is presented. The detailed derivation of the coarse-graining on different levels shows transparently the approximations involved. This allows straight-forward assessment of the capability, validity, and applicability of various schemes for modeling the electrochemical interfaces. The performed derivation enables also the removal of the coarse-graining if needed; this freedom can be utilized to study, e.g.,, nuclear tunneling and specific adsorption at a fixed electrode potential. Another specific example of the general applicability of the theory is an extension to treat adiabatic and nonadiabatic electron transfer kinetics as a function of the electron and ion chemical potentials currently under development by us.

On the simplest level of theory, the presented coarse-graining provides a well-defined approach to continuum solvent models and Poisson-Boltzmann models of the ionic double layer. To compare different continuum models, several mPB models, including the Stern layer, finite-size effects, and dielectric decrement, were implemented in the GPAW code and tested. As detailed, other mPB models can be motivated and implemented by using functional minimization of the DFT grand free energy functional. We present an extensive discussion and development of simulating charged systems in contact with a continuum dielectric and mPB double-layer.

The tested mPB models vary from simple homogeneous jellium models[33] and neutralizing Gaussian background charges to common point-like PB and to mPB models with specific ion contributions including the ion size and dielectric decrement effects. All the included mPB approaches are based on the linear dielectric SCMVD[59] model of the liquid. Calculations for the interfacial electrostatic potential distributions show that the jellium model screens less than other mPB models, while the mPB models apart from ionic decrement produce almost identical electrostatic potentials. The ionic decrement model screens the charge rather slowly but introduces slight asymmetry between positive and negative potentials. The long-range behavior of the ESM[16]-like boundary condition method differs significantly from the mPB models.

Computed double-layer capacitance profiles for Au(210) in a NaF electrolyte show that the mPB models with a linear dielectric are incapable of capturing the shape of experimentally determined double layer capacitance curve even when several factors accounting for ion-specific effects are accounted for. All the utilized mPB models including linearized, point-like Gouy-Chapmann, finite-ion Bikerman-Freise, and the ion decrement model yield almost constant double layer capacitances rather than an experimentally obtained bell-shaped capacitance within the

tested potential range in a 0.5M NaF solution. Furthermore, the absolute capacitance values are very sensitive to the details on the underlying solvent cavity.

Thus, the overall outcome is that a linear dielectric model even when combined with more complex mPB electrolyte description cannot qualitatively reproduce the experimentally measured capacitance; at this level, already jellium-like electrolytes result in almost identical double-layer capacitances and interfacial electrostatic potential similar to the more complicated mPB models. On the other hand, non-linear continuum solvents[32] have shown promising results for describing the double-layer capacitance.[37]

Our results show that even addition of ion-specific interactions into simple continuum electrolyte models is unable to provide a fully satisfactory description of electrolyte-electrode interfaces. Instead, approaches beyond linear dielectric continuum models such as including explicit solvent molecules/ions or the dipolar response of the liquid to external potentials should be investigated. The presented theoretical framework allows a natural way to include important interactions within GC-DFT and to develop better computational models for electrocatalysis. Finally, while we have presented a rigorous and well-defined GC-DFT coarse-graining scheme and applied it to continuum electrolytes, there are serious caveats that need to be recognized and addressed as the use of linear continuum models for modeling the electrochemical interfaces keeps increasing.

SUPPLEMENTARY MATERIAL

See supplementary material for the (1) experimentally measured differential capacitance of Au(210) in NaF solutions, (2) general structure of canonical electronic DFT and Helmholtz free energy, (3) general structure of joint DFT, (4) derivation of modified Poisson-Boltzmann equations, (5) details of original SCMVD method, (6) calculation details for obtaining the cavity parameters from AIMD, (7) differential capacitance plots, (8) implementation details of the boundary condition method, and (9) list of symbols.

ACKNOWLEDGMENTS

REFERENCES

[1]A. J. Bard and L. R. Faulker, *Electrochemical Methods: Fundamentals and Applications*, 2nd ed. (John Wiley and Sons, Inc., 2001).
[2]R. Jinnouchi, K. Kodama, and Y. Morimoto, "Electronic structure calculations on electrolyte–electrode interfaces: Successes and limitations," Curr. Opin. Electrochem. **8**, 103 (2018).

[3]M. Tuckerman, *Statistical Mechanics: Theory and Molecular Simulations* (Oxford University Press, 2010).

[4]J. Cheng, X. Liu, J. VandeVondele, M. Sulpizi, and M. Sprik, "Redox potentials and acidity constants from density functional theory based molecular dynamics," Acc. Chem. Res. **47**(12), 3522–3529 (2014).

[5]T. Ikeshoji and M. Otani, "Toward full simulation of the electrochemical oxygen reduction reaction on pt using first-principles and kinetic calculations," Phys. Chem. Chem. Phys. **19**, 4447–4453 (2017).

[6]N. Holmberg and K. Laasonen, "*Ab initio* electrochemistry: Exploring the hydrogen evolution reaction on carbon nanotubes," J. Phys. Chem. C **119**(28), 16166–16178 (2015).

[7]J.-P. Hansen and J.-P. Hansen, *Theory of Simple Liquids*, 3rd ed. (Academic Press, 2006).

[8]J. Forsman, C. E. Woodward, and R. Szparaga, *Computational Electrostatics for Biological Applications* (Springer International Publishing, 2015).

[9]T. J. Sluckin, "Applications of the density-functional theory of charged fluids," J. Chem. Soc., Faraday Trans. 2 **77**, 575–586 (1981).

[10]N. David Mermin, "Thermal properties of the inhomogeneous electron gas," Phys. Rev. **137**, A1441–A1443 (1965).

[11]A. Pribram-Jones, S. Pittalis, E. K. U. Gross, and K. Burke, "Thermal density functional theory in context," in *Frontiers and Challenges in Warm Dense Matter*, edited by F. Graziani, M. P. Desjarlais, R. Redmer, and S. B. Trickey (Springer International Publishing, 2014), pp. 25–60.

[12]S. A. Petrosyan, A. A. Rigos, and T. A. Arias, "Joint density-functional theory: *Ab initio* study of Cr_2O_3 surface chemistry in solution," J. Phys. Chem. B **109**(32), 15436–15444 (2005).

[13]A. Kovalenko and F. Hirata, "Self-consistent, Kohn-Sham DFT and three-dimensional RISM description of a metal-molecular liquid interface," J. Mol. Liq. **90**(1), 215–224 (2001).

[14]A. Kovalenko and S. Gusarov, "Multiscale methods framework: Self-consistent coupling of molecular theory of solvation with quantum chemistry, molecular simulations, and dissipative particle dynamics," Phys. Chem. Chem. Phys. **20**, 2947–2969 (2018).

[15]S. Nishihara and M. Otani, "Hybrid solvation models for bulk, interface, and membrane: Reference interaction site methods coupled with density functional theory," Phys. Rev. B **96**, 115429 (2017).

[16]M. Otani and O. Sugino, "First-principles calculations of charged surfaces and interfaces: A plane-wave nonrepeated slab approach," Phys. Rev. B **73**, 115407 (2006).

[17]N. Bonnet, T. Morishita, O. Sugino, and M. Otani, "First-principles molecular dynamics at a constant electrode potential," Phys. Rev. Lett. **109**, 266101 (2012).

[18]R. Sundararaman, W. A. Goddard III, A. Tomas, and Arias, "Grand canonical electronic density-functional theory: Algorithms and applications to electrochemistry," J. Chem. Phys. **146**(11), 114104 (2017).

[19]T. Kreibich, R. van Leeuwen, and E. K. U. Gross, "Multicomponent density-functional theory for electrons and nuclei," Phys. Rev. A **78**, 022501 (2008).

[20]S. Smidstrup, D. Stradi, J. Wellendorff, P. A. Khomyakov, U. G. Vej-Hansen, M.-E. Lee, and T. Ghosh, E. Jónsson, H. Jónsson, and K. Stokbro, "First-principles Green's-function method for surface calculations: A pseudopotential localized basis set approach," Phys. Rev. B **96**, 195309 (2017).

[21]C. D. Taylor, S. A. Wasileski, J.-S. Filhol, and M. Neurock, "First principles reaction modeling of the electrochemical interface: Consideration and calculation of a tunable surface potential from atomic and electronic structure," Phys. Rev. B **73**, 165402 (2006).

[22]J. D. Goodpaster, A. T. Bell, and M. Head-Gordon, "Identification of possible pathways for C–C bond formation during electrochemical reduction of CO_2: New theoretical insights from an improved electrochemical model," J. Phys. Chem. Lett. **7**(8), 1471–1477 (2016).

[23]R. Jinnouchi and A. B. Anderson, "Electronic structure calculations of liquid-solid interfaces: Combination of density functional theory and modified Poisson-Boltzmann theory," Phys. Rev. B **77**, 245417 (2008).

[24]E. Skúlason, V. Tripkovic, M. E. Bjørketun, S. Gudmundsdóttir, G. Karlberg, J. Rossmeisl, T. Bligaard, H. Jónsson, and J. K. Nørskov, "Modeling the electrochemical hydrogen oxidation and evolution reactions on the basis of density functional theory calculations," J. Phys. Chem. C **114**(42), 18182–18197 (2010).

[25]K. Letchworth-Weaver and T. A. Arias, "Joint density functional theory of the electrode-electrolyte interface: Application to fixed electrode potentials, interfacial capacitances, and potentials of zero charge," Phys. Rev. B **86**, 075140 (2012).

[26]Y.-H. Fang and Z.-P. Liu, "Mechanism and Tafel lines of electro-oxidation of water to oxygen on $RuO_2(110)$," J. Am. Chem. Soc. **132**(51), 18214–18222 (2010).

[27]I. Dabo, B. Kozinsky, N. E. Singh-Miller, and N. Marzari, "Electrostatics in periodic boundary conditions and real-space corrections," Phys. Rev. B **77**, 115139 (2008).

[28]O. Andreussi and N. Marzari, "Electrostatics of solvated systems in periodic boundary conditions," Phys. Rev. B **90**, 245101 (2014).

[29]S. Ringe, H. Oberhofer, and K. Reuter, "Transferable ionic parameters for first-principles Poisson-Boltzmann solvation calculations: Neutral solutes in aqueous monovalent salt solutions," J. Chem. Phys. **146**(13), 134103 (2017).

[30]G. Fisicaro, L. Genovese, O. Andreussi, N. Marzari, and S. Goedecker, "A generalized Poisson and Poisson-Boltzmann solver for electrostatic environments," J. Chem. Phys. **144**(1), 014103 (2016).

[31]K. Mathew and R. G. Hennig, "Implicit self-consistent description of electrolyte in plane-wave density-functional theory," e-print arXiv:1601.03346 (2016).

[32]D. Gunceler, K. Letchworth-Weaver, R. Sundararaman, K. A. Schwarz, and T. A. Arias, "The importance of nonlinear fluid response in joint density-functional theory studies of battery systems," Modell. Simul. Mater. Sci. Eng. **21**(7), 074005 (2013).

[33]G. Kastlunger, P. Lindgren, and A. A. Peterson, "Controlled-potential simulation of elementary electrochemical reactions: Proton discharge on metal surfaces," J. Phys. Chem. C **122**(24), 12771–12781 (2018).

[34]G. Fisicaro, L. Genovese, O. Andreussi, S. Mandal, N. N. Nair, N. Marzari, and S. Goedecker, "Soft-sphere continuum solvation in electronic-structure calculations," J. Chem. Theory Comput. **13**(8), 3829–3845 (2017).

[35]O. Andreussi, I. Dabo, and N. Marzari, "Revised self-consistent continuum solvation in electronic-structure calculations," J. Chem. Phys. **136**(6), 064102 (2012).

[36]R. Sundararaman and K. Schwarz, "Evaluating continuum solvation models for the electrode-electrolyte interface: Challenges and strategies for improvement," J. Chem. Phys. **146**(8), 084111 (2017).

[37]R. Sundararaman, K. Letchworth-Weaver, and K. A. Schwarz, "Improving accuracy of electrochemical capacitance and solvation energetics in first-principles calculations," J. Chem. Phys. **148**(14), 144105 (2018).

[38]J. F. Capitani, R. F. Nalewajski, and R. G. Parr, "Non–Born–Oppenheimer density functional theory of molecular systems," J. Chem. Phys. **76**(1), 568–573 (1982).

[39]K. Chan and J. K. Nørskov, "Electrochemical barriers made simple," J. Phys. Chem. Lett. **6**(14), 2663–2668 (2015).

[40]E. A. Guggenheim, *Thermodynamics: An Advanced Treatment for Chemists and Physicists* (North Holland Physics Publishing, 1967).

[41]D. Petz, "Entropy, von Neumann and the von Neumann entropy," e-print arXiv:math-ph/0102013v1 (2001).

[42]M. Levy, "Electron densities in search of Hamiltonians," Phys. Rev. A **26**, 1200–1208 (1982).

[43]A. Migliore, N. F. Polizzi, M. J. Therien, and D. N. Beratan, "Biochemistry and theory of proton-coupled electron transfer," Chem. Rev. **114**(7), 3381–3465 (2014).

[44]A. Nitzan, *Chemical Dynamics in Condensed Phases: Relaxation, Transfer, and Reactions in Condensed Molecular Systems* (Oxford University Press, 2006).

[45]R. Crespo-Otero and M. Barbatti, "Recent advances and perspectives on nonadiabatic mixed quantum–classical dynamics," Chem. Rev. **118**(15), 7026–7068 (2018).

[46]M. V. Pak, A. Chakraborty, and S. Hammes-Schiffer, "Density functional theory treatment of electron correlation in the nuclear electronic orbital approach," J. Phys. Chem. A **111**(20), 4522–4526 (2007).

[47]J. Wu, *Classical Density Functional Theory for Molecular Systems* (Springer Singapore, Singapore, 2017), pp. 65–99.

[48]W. Schmickler and R. Guidelli, "The partial charge transfer," Electrochim. Acta **127**, 489–505 (2014).

[49]L. D. Chen, M. Bajdich, J. M. P. Martirez, C. M. Krauter, J. A. Gauthier, E. A. Carter, A. C. Luntz, K. Chan, and J. K. Nørskov, "Understanding the apparent fractional charge of protons in the aqueous electrochemical double layer," Nat. Commun. **9**(1), 3202 (2018).

[50]R. de Levie, "The electrosorption valency and partial charge transfer," J. Electroanal. Chem. **562**(2), 273–276 (2004).

[51]M. Franco-Perez, P. W. Ayers, J. L. Gazquez, and A. Vela, "Local chemical potential, local hardness, and dual descriptors in temperature dependent chemical reactivity theory," Phys. Chem. Chem. Phys. **19**, 13687–13695 (2017).

[52]R. Haase, *Thermodynamics of Irreversible Processes* (Addison-Wesley, 1969).

[53]O. Anatole von Lilienfeld and M. E. Tuckerman, "Molecular grand-canonical ensemble density functional theory and exploration of chemical space," J. Chem. Phys. **125**(15), 154104 (2006).

[54]C. R. Jacob and J. Neugebauer, "Subsystem density functional theory," Wiley Interdisc. Rev.: Comput. Mol. Sci. **4**(4), 325–362 (2014).

[55]A. Patrykiejew, S. Sokolowski, and O. Pizio, *Statistical Surface Thermodynamics*, edited by K. Wandelt (Wiley-Blackwell, 2016), Chap. 46, pp. 883–1253.

[56]L. Mier-y-Teran, S. H. Suh, H. S. White, and H. T. Davis, "A nonlocal free-energy density–functional approximation for the electrical double layer," J. Chem. Phys. **92**(8), 5087–5098 (1990).

[57]J. D. Jackson, *Classical Electrodynamics*, 3rd ed. (Wiley, 1998).

[58]D. J. Bonthuis and R. R. Netz, "Beyond the continuum: How molecular solvent structure affects electrostatics and hydrodynamics at solid–electrolyte interfaces," J. Phys. Chem. B **117**(39), 11397–11413 (2013).

[59]A. Held and M. Walter, "Simplified continuum solvent model with a smooth cavity based on volumetric data," J. Chem. Phys. **141**(17), 174108 (2014).

[60]Y. Nakayama and D. Andelman, "Differential capacitance of the electric double layer: The interplay between ion finite size and dielectric decrement," J. Chem. Phys. **142**(4), 044706 (2015).

[61]D. Ben-Yaakov, D. Andelman, and R. Podgornik, "Dielectric decrement as a source of ion-specific effects," J. Chem. Phys. **134**(7), 074705 (2011).

[62]N. Gavish and K. Promislow, "Dependence of the dielectric constant of electrolyte solutions on ionic concentration: A microfield approach," Phys. Rev. E **94**, 012611 (2016).

[63]M. Z. Bazant, M. Sabri Kilic, B. D. Storey, and A. Ajdari, "Towards an understanding of induced-charge electrokinetics at large applied voltages in concentrated solutions," Adv. Colloid Interface Sci. **152**(1), 48–88 (2009).

[64]I. Borukhov, D. Andelman, and H. Orland, "Steric effects in electrolytes: A modified Poisson-Boltzmann equation," Phys. Rev. Lett. **79**, 435–438 (1997).

[65]E. Gongadze, A. Velikonja, S. Perutkova, P. Kramar, A. Macek-Lebar, V. Kralj-Iglic, and A. Iglic, "Ions and water molecules in an electrolyte solution in contact with charged and dipolar surfaces," Electrochim. Acta **126**, 42–60 (2014).

[66]F. Booth, "The dielectric constant of water and the saturation effect," J. Chem. Phys. **19**(4), 391–394 (1951).

[67]S. Trasatti, "The absolute electrode potential: An explanatory note (recommendations 1986)," J. Electroanal. Chem. Interfacial Electrochem. **209**(2), 417–428 (1986).

[68]S. Trasatti, "The 'absolute' electrode potential–The end of the story," Electrochim. Acta **35**(1), 269–271 (1990).

[69]K. Leung, "Surface potential at the air–water interface computed using density functional theory," J. Phys. Chem. Lett. **1**(2), 496–499 (2010).

[70]M. Otani, I. Hamada, O. Sugino, Y. Morikawa, Y. Okamoto, and T. Ikeshoji, "Electrode dynamics from first principles," J. Phys. Soc. Jpn. **77**(2), 024802 (2008).

[71]M. N. Tamashiro and H. Schiessel, "Where the linearized Poisson–Boltzmann cell model fails: Spurious phase separation in charged colloidal suspensions," J. Chem. Phys. **119**(3), 1855–1865 (2003).

[72]B. Zoetekouw and R. van Roij, "Volume terms for charged colloids: A grand-canonical treatment," Phys. Rev. E **73**, 021403 (2006).

[73]F. G. Donnan, "The theory of membrane equilibria," Chem. Rev. **1**(1), 73–90 (1924).

[74]L. Wan, S. Xu, M. Liao, C. Liu, and P. Sheng, "Self-consistent approach to global charge neutrality in electrokinetics: A surface potential trap model," Phys. Rev. X **4**, 011042 (2014).

[75]A. Baskinz and D. Prendergast, "Improving continuum models to define practical limits for molecular models of electrified interfaces," J. Electrochem. Soc. **164**, E3438–E3447 (2017).

[76]A. R. Denton, "Charge renormalization, effective interactions, and thermodynamics of deionized colloidal suspensions," J. Phys.: Condens. Matter **20**(49), 494230 (2008).

[77]J. S. Hub, B. L. de Groot, H. Grubmüller, and G. Groenhof, "Quantifying artifacts in Ewald simulations of inhomogeneous systems with a net charge," J. Chem. Theory Comput. **10**(1), 381–390 (2014).

[78]J. J. Mortensen, L. B. Hansen, and K. W. Jacobsen, "Real-space grid implementation of the projector augmented wave method," Phys. Rev. B **71**, 035109 (2005).

[79]J. Enkovaara, C. Rostgaard, J. J. Mortensen, J. Chen, M. Dułak, L. Ferrighi, J. Gavnholt, C. Glinsvad, V. Haikola, H. A. Hansen, H. H. Kristoffersen, M. Kuisma, A. H. Larsen, L. Lehtovaara, M. Ljungberg, O. Lopez-Acevedo, P. G. Moses, J. Ojanen, T. Olsen, V. Petzold, N. A. Romero, J. Stausholm-Møller, M. Strange, G. A. Tritsaris, M. Vanin, M. Walter, B. Hammer, H. Häkkinen, G. K. H. Madsen, R. M. Nieminen, J. K. Nørskov, M. Puska, T. T. Rantala, J. Schiøtz, K. S. Thygesen, and K. W. Jacobsen, "Electronic structure calculations with GPAW: A real-space implementation of the projector augmented-wave method," J. Phys.: Condens. Matter **22**(25), 253202 (2010).

[80]L. Bengtsson, "Dipole correction for surface supercell calculations," Phys. Rev. B **59**, 12301–12304 (1999).

[81]P. E. Blöchl, "Projector augmented-wave method," Phys. Rev. B **50**, 17953–17979 (1994).

[82]A. H. Larsen, J. J. Mortensen, J. Blomqvist, I. E. Castelli, R. Christensen, M. Dułak, J. Friis, M. N. Groves, B. Hammer, C. Hargus, E. D. Hermes, P. C. Jennings, P. Bjerre Jensen, J. Kermode, J. R. Kitchin, E. L. Kolsbjerg, J. Kubal, K. Kaasbjerg, S. Lysgaard, J. Bergmann Maronsson, T. Maxson, T. Olsen, L. Pastewka, A. Peterson, C. Rostgaard, J. Schiøtz, O. Schütt, M. Strange, K. S. Thygesen, T. Vegge, L. Vilhelmsen, M. Walter, Z. Zeng, and K. W. Jacobsen, "The atomic simulation environment–A Python library for working with atoms," J. Phys.: Condens. Matter **29**(27), 273002 (2017).

[83]J. P. Perdew, K. Burke, and M. Ernzerhof, "Generalized gradient approximation made simple," Phys. Rev. Lett. **77**, 3865–3868 (1996).

[84]A. Bondi, "van der Waals volumes and radii," J. Phys. Chem. **68**(3), 441–451 (1964).

[85]S. S. Batsanov, "van der Waals radii of elements," Inorg. Mater. **37**(9), 871–885 (2001).

[86]A. Gross, *Theory of Solid/Electrolyte Interfaces*, Psi-k Highlight No. 125 (Wiley, 2014).

[87]R. I. Slavchov, J. K. Novev, T. V. Peshkova, and N. A. Grozev, "Surface tension and surface $\Delta\chi$-potential of concentrated Z_+:Z_- electrolyte solutions," J. Colloid Interface Sci. **403**, 113–126 (2013).

[88] A. Hamelin, Z. Borkowska, and J. Stafiej, "A double layer study of the (210) and (111) faces of gold in aqueous nabf4 solutions," J. Electroanal. Chem. Interfacial Electrochem. **189**(1), 85–97 (1985).

[89] J. Rossmeisl, E. Skúlason, M. E. Bjørketun, V. Tripkovic, and J. K. Nørskov, "Modeling the electrified solid–liquid interface," Chem. Phys. Lett. **466**(1-3), 68–71 (2008).

[90] A. Hamelin, "Study of the (210) face of gold in aqueous solutions," J. Electroanal. Chem. Interfacial Electrochem. **138**(2), 395–400 (1982).

[91] S. Trasatti, "Surface science and electrochemistry: Concepts and problems," in *Proceedings of the IUVSTA Workshop on Surface Science and Electrochemistry* [Surf. Sci. **335**, 1–9 (1995)].